This Page Is Inserted by IFW Operations
and is not a part of the Official Record

BEST AVAILABLE IMAGES

Defective images within this document are accurate representations of the original documents submitted by the applicant.

Defects in the images may include (but are not limited to):

- BLACK BORDERS
- TEXT CUT OFF AT TOP, BOTTOM OR SIDES
- FADED TEXT
- ILLEGIBLE TEXT
- SKEWED/SLANTED IMAGES
- COLORED PHOTOS
- BLACK OR VERY BLACK AND WHITE DARK PHOTOS
- GRAY SCALE DOCUMENTS

IMAGES ARE BEST AVAILABLE COPY.

As rescanning documents *will not* correct images, please do not report the images to the Image Problem Mailbox.

REMARKS

Claim 17 is canceled without prejudice or disclaimer. Accordingly, upon entry of the instant response, Claims 11-16 and 18-27 will be pending.

The specification is amended to add the US Patent Number that issued from US Application Serial No. 09/371,056. Thus, Applicant respectfully requests withdrawal of the objection to the specification.

Claims 14 and 15 stand objected to as being dependent from rejected Claim 11. Applicant respectfully requests clarification as claim 11 is rejected, not canceled. Further, all of the remaining pending claims depend from claim 11 as well, however, only claims 14 and 15 are objected.

Claim 17 is rejected under 35 U.S.C. 112, first paragraph. Claim 17 is canceled above. Thus, this rejection may be withdrawn.

Claims 11-13 and 16-27 are rejected under 35 U.S.C. 112, first paragraph as the specification has not been found to enable any person skilled in the art to which it pertains, or with which it is most nearly connected, to make and use the invention commensurate in scope with these claims. The rejection of Claims 11-13, 16, and 18-27 is respectfully traversed on ground of the discussion below. Applicant notes that Claim 17 is canceled.

Submitted herewith is a copy of Notheis, C. et al., BBA, Vol.1247, pages 265-271 (1995) (copy enclosed for the Examiner's convenience) which discloses the purification and characterization of the pyridoxal-5'-phosphate:oxygen oxidoreductase from *E. coli* (gi:148095). Overexpression and purification of the *E.coli* enzyme show that the enzyme is a FMN-containing protein that specifically oxidizes pyridoxal phosphate and pyridoxamine phosphate. Also submitted herewith is Appendix A which provides a comparison of the claimed sequence with the *E. coli* PNPox and the *M. xanthus* frpA gene product (which has also been shown to bind FMN tightly). FMN binding is an expected property for PNP oxidase from the enzymological characterization of the purified eukaryotic and activities in crude extracts of *E.coli* (Lam et al., J. Bacteriol. Vol: 174; 6033-6045, 1992, previously submitted and copy enclosed for the Examiner's convenience)). This comparison demonstrates the sequence of the invention possesses stretches of highly conserved regions. One skilled in the art would have appreciated that the more highly conserved a residue is, the less likely that it could be modified and function maintained. From this alignment in Appendix A, one could quickly determine which amino acid residues might be modified in SEQ ID NO:10 without a likely change in function. Since SEQ ID NOs:10 and the *E.coli* sequence share 40% identity, one of skill in the art would have appreciated that many variants sharing at least 80%

sequence identity to the SEQ ID NO:10 would have been expected to retain PNPox activity. This has been further supported recently by the elucidation of active site structure of the *E.coli* PNPox (di Salvo, JMB, Vol: 315, 385-397 (2002), copy enclosed for the Examiner's convenience). The authors disclose specific residues in the protein sequence, which enable interaction with the PNP phosphate moiety. For the Examiner's convenience the residues which enable such interaction are underlined in the alignment in Appendix A. All of the residues are highly conserved among the *E.coli*, the *M. xanthus* and the claimed sequence.

In view of the foregoing remarks, one skilled in the art would know how to use the claimed sequence without undue experimentation and that the rejection according to 35 USC §112, first paragraph, should be withdrawn.

For the foregoing reasons, Applicants respectfully request reconsideration and allowance of claims 11-16 and 18-27.

Please charge any requisite fee or credit any overpayment to Deposit Account No. 04-1928 (E. I. du Pont de Nemours and Company).

Respectfully submitted,

Lori Y. Beardell

LORI Y. BEARDELL
ATTORNEY FOR APPLICANTS
REGISTRATION NO. 34,293
TELEPHONE: (302) 992-4926
FACSIMILE: (302) 892-1026

Dated: Aug. 6, 2003

APPENDIX A

Comparison of the amino acid sequences of the Pyridoxamine 5'-phosphate oxidase from corn clone contig with SID No's: csin.pk0050.f8, cr1n.pk0063.f3, and cbn10.pk0048.g12 (SEQ ID NO:10), the M.xanthus frpA set forth NCBI General Identifier No. 20800466 and E. coli PNPox set forth in NCBI General Identifier No. 148095. Amino acids conserved among the E.coli PNPox and Seq ID NO: 10 or all three sequences are indicated with a single or double asterix above the conserved residues, respectively. Dashes are used by the program to maximize alignment of the sequences. Residues that have been shown to play an important role in the catalytic activity of Pyridoxamine 5'-phosphate (di Salvo et al.(2002) J.Mol.Biol 315, 385-397) are underlined.

```
                 *
                 *                    ** *                    **          *  **        *
SEQ_ID_NO:10     MLVSLTAPKLCAKKFTGPHHFLGGXFVPPPILNQLRDFSSSFTLGTSMCVRIGKAPSVEI
gi:20800466      M------AQRGKRGGEGPGHVPQAPRLGER--GHLRGDEEDIHVRTLTCVPDESTAKVHT
gi:148095        M------SDND--------ELQQIAHL-RR--EYTKGG----------------------

                          *        **    *       *  *       * **    *     * *  *
                    *     *        **    *   *   *  *       ****    *     * *  *
SEQ_ID_NO:10     SSLRENYISPELLESQVMSDPFDQFLKWFDEAVTAGPGLREPNAMALTTANKEGKPSSRM
gi:20800466      C--RAPFM---LHRVMIPPDPIQRFAELFERAKQA--IAVDPNAMVVATVGDDGRPSARV
gi:148095        ----------LRRRDLPADPLTLFERWLSQACEA-KLADPTAMVVATVDEHGQPYQRI

                 ****  *  * * ***  ***         *   * * *      ** * *  *      *
                 ****  *  * * ***  ***         * *** ***      ****** ** *    * *
SEQ_ID_NO:10     VLLKGVDKQGFVWYTNYGSRKAHDLCENPNAALLFYWNEMNRQVRVEGSVEKVPEAESDK
gi:20800466      VLLKDFDARGFVFYTNHESRKGREARAHPYAALCFYWQPLNEQVRVEGRVERVTDAEADA
gi:148095        VLLKHYDEKGMVFYTNLGSRKAHQIENNPRVSLLFPWHTLERQVMVIGKAERLSTLEVMK

                 ** ** * ** **  * **      *  *        ***        * *  * *
                 ** ** **** **  * **   * ** *        ****       * *  * *    *
SEQ_ID_NO:10     YFHSRPRGSQLGAIVSKQSTVIAGREVLQQDYKKLEQKYSDGSLIPKPEYWGGYKLTPTL
gi:20800466      YFQSRARGSQVGAWASLQSQPLATREELEARVAEVEQKYAGQP-VPRPPHWSGFRVVPDR
gi:148095        YFHSRPRDSQIGAWVSKQSSRISARGILESKFLELKQKFQQGE-VPLPSFWGGFRVSLEQ

                  ***      *****  *  **       *    *  *
                  ***   * ******  *  **  *    *    *  *
SEQ_ID_NO:10     FEFWQGQQSRLHDRLQYSQREVDGSTVWHIERLS-P
gi:20800466      IEFWHAQESRLHDRHVY-LREDGG---WRTQMLY-P
gi:148095        IEFWQGGEHRLHDRFLY-QRENDA---WKIDRLA-P
```

JUN-16-2003 MON 01:00 PM PIONEER HI BRED FAX NO. 2532184 BB1201 P. 02

Notice: This material may be protected by copyright

ELSEVIER

Biochimica et Biophysica Acta 1247 (1995) 265–271

BBA Biochimica et Biophysica Acta

Purification and characterization of the pyridoxol-5′-phosphate:oxygen oxidoreductase (deaminating) from *Escherichia coli*

Caroline Notheis, Christel Drewke, Eckhard Leistner *

Institut für Pharmazeutische Biologie, Rheinische Friedrich-Wilhelms-Universität, Nussallee 6, D-53115 Bonn, Germany

Received 23 September 1994; accepted 1 November 1994

Abstract

The *E. coli* gene *pdxH* encoding pyridoxol-5′-phosphate:oxygen oxidoreductase (deaminating) (EC 1.4.3.5, PdxH) was cloned, located to phage 20B5 of the library of Kohara et al. (Kohara, Y., Akiyama, K. and Isono K. (1987) Cell 50, 495–508) and assigned to a stretch between 36.0 and 36.1 min of the *E. coli* chromosome. The gene was overexpressed as a MBP/PdxH fusion protein. The fusion protein was purified by affinity chromatography on an amylose resin and hydrolyzed in the presence of protease 'factor Xa' resulting in homogeneous PdxH protein after another column chromatography. Both the MBP/PdxH fusion protein and the PdxH protein were characterized. Both enzymes are FMN-dependent enzymes which oxidize pyridoxol phosphate and pyridoxamine phosphate in the presence of oxygen to pyridoxal phosphate. K_m values of both proteins were similar ranging from 350 to 400 μM for the two substrates. The enzymes did not accept non-phosphorylated substrates. Kinetic data indicate that the enzyme (MBP/PdxH) is product inhibited (K_i 8 μM) by pyridoxal phosphate as a mixed type inhibitor. As revealed by gel exclusion chromatography a minor fraction of the fusion protein formed a dimer, whereas the bulk amount of protein was a monomer. No indication was found that the PdxH protein forms a dimer. The monomer was shown to be catalytically active.

Keywords: Vitamin B-6; Pyridoxol phosphate oxidase; Pyridoxamine phosphate oxidase; (*E. coli*)

1. Introduction

Pyridoxol (pyridoxamine) phosphate oxidase (EC 1.4.3.5) catalyzes the terminal step in the biosynthesis of pyridoxal phosphate. The enzyme has been detected in rabbit liver [2,3], brain [4], red cells [5], yeast [6] and bacteria [7–9]. The enzyme catalyzes the oxidation of either pyridoxine phosphate or pyridoxamine phosphate [10] and *N*-(5′-phospho-4′-pyridoxyl)amine [11] in the presence of oxygen. The properties of the enzyme isolated from different sources are similar. The enzyme forms a homodimer with the monomer molecular weight ranging from M_r 27 000 to 30 000. One dimer harbours a single FMN. The properties of the bacterial enzyme are relatively little explored, the gene encoding the pyridoxol phosphate oxidase from *E. coli*, however, has been sequenced recently [12].

This made it possible to purify and overexpress the enzyme and to test predictions which are based on the known nucleotide sequence of the gene. Thus, the *E. coli* pyridoxol phosphate oxidase is likely to bind FMN, as indicated by its full length homology with the FMN binding Fpr protein of *Myxococcus xanthus* [12]. We have overexpressed the pyridoxol phosphate oxidase (PdxH) as a fusion protein (MBP/PdxH) and purified the enzyme to homogeneity by affinity chromatography. Our data show that the enzyme is a FMN containing protein that oxidizes pyridoxol phosphate and pyridoxamine phosphate, whereas non-phosphorylated B-6 vitamers (such as pyridoxamin or pyridoxol) do not function as substrates. The *pdxH* gene was located to the 20B5 phage of Kohara et al. [1] by complementation studies indicating that *pdxH* maps between 36.0 to 36.1 min of the *E. coli* chromosome. Our data also show that the sequence published by Lam and Winkler [12] and the 20B5 phage of Kohara et al. [1] indeed encode pyridoxol-5′-phosphate:oxygen oxidoreductase (deaminating) (EC 1.4.3.5).

Abbreviations: MBP, maltose binding protein; SDS-PAGE, sodium dodecyl sulfate polyacrylamide electrophoresis; PdxH, pyridoxol-5′-phosphate:oxygen oxidoreductase (deaminating) (EC 1.4.3.5).

* Corresponding author. Fax: +49 228 733250.

0167-4838/95/$09.50 © 1995 Elsevier Science B.V. All rights reserved
SSDI 0167-4838(94)00235-5

JUN-16-2003 MON 01:01 PM PIONEER HI BRED FAX NO. 2532184 P. 04

Notice: This material may be protected by copyright

2. Materials and methods

2.1. Strains

Escherichia coli WG2 (*pdxH*$^-$) as described by Dempsey [13] was obtained from Dr. I.D. Spenser, Hamilton, Ontario, Canada. *E. coli* XL1 blue (*recA1*, *endA1*, *gyrA96*, *thi-1*, *hsdR17*, *supE44*, *relA1*, *lac*, [*F'proAB*, *lacI*^{q}*ΔZM15*, *Tn10*(*tet*^{r})] was from Stratagene, Heidelberg, Germany. pMAL-c2 (*Ap*^{r}, *lacI*^{q}, P_{tac}/*malE-lacPOZ'*) was from New England Biolabs, Schwalbach, Germany.

Taq-DNA polymerase was from Stratagene, Heidelberg, Germany. Pyridoxal phosphate and pyridoxamine phosphate (HCl) were from Sigma, Deisenhofen, Germany, whereas pyridoxol phosphate was prepared following the method of Tschopp and Kirschner [14].

2.2. Growth of strains

One liter of Rich medium (10 g Bacto-Trypton, 5 g yeast extract, 5 g NaCl, 2 g glucose, 75 mg/ml ampicillin) was inoculated (1% inoculum) with a preculture and incubated at 310 K in an Infors shaker (150 rpm) until an OD_{600} of 0.5 was reached. To induce the expression of MBP'/PdxH, IPTG (final conc. 0.3 mM) was added 2 h before harvest. Cells were collected by centrifugation (4000 × *g*, 20 min).

2.3. Construction of pMAL-c2 / pdxH

The *pdxH* gene was generated by PCR using primers C1 (5'-TAAAGGAATTCATGTCTGATAACGA-3') and C2 (5'CTAAAGTTCTAGAATCAGGAGAGTA-3') and genomic DNA from *E. coli* K12.

The primers were derived from the sequence published by Lam and Winkler [12] in order to prime an amplification product harbouring the whole *pdxH* coding sequence. They were constructed to yield a PCR product containing an *Eco*RI restriction site at the 5' and an *Xba*I site at the 3' noncoding region. Amplification was carried out in a Trio-Thermoblock (Biometra, Göttingen, Germany) using recombinant *Taq* polymerase according to the suppliers' recommendation (Stratagene, Heidelberg, Germany). Thirty-five cycles were carried out, each cycle consisting of denaturation at 367 K (30 s), annealing at 325 K (50 s), and extension at 345 K (1 min). The PCR products were checked on an agarose gel. Recombinant plasmids were constructed by standard techniques [15] using the vector's *Eco*RI and *Xba*I sites for cloning. After transformation into *E. coli* XL1 blue the recombinant pMAL-c2 plasmid was isolated and the *pdxH* gene sequenced using the method of Sanger [16]. The following sequencing primers were employed: C5 (5'-AACCTCGGGATCGAGGGAA-3') and C6 (5'-GAATCAGGAGTACCAGCGAT-3').

The sequence was found to be identical to Lam and Winkler's [12] published sequence indicating that the *Taq* polymerase had not introduced a mismatch.

The vector pMAL-c2 contains a sequence coding for the recognition site of the specific proteinase 'factor Xa'. This allows MBP to be separated from the PdxH protein. Between the sequence coding for the proteinase recognition site and the ATG-start codon of *pdxH* there is a vector derived sequence of 12 base pairs. Thus, after hydrolysis of the MBP/PdxH fusion protein with proteinase 'factor Xa', PdxH is linked to a peptide consisting of 4 additional amino acids (Ile, Ser, Glu, Phe).

2.4. Purification of PdxH

Bacterial cells (5 g wet mass) harbouring pMAL-c2/*pdxH* were suspended in buffer (50 ml, 20 mM Tris-HCl, 200 mM NaCl, 1 mM EDTA, 1 mM NaN_3, 1 mM dithiothreitol, pH 7.4) and frozen (253 K). Before ultrasonic treatment (Branson sonifier, Danbury, USA; 10-times 20 s, 50% output at stage 5) cells were thawed at 277 K (water bath). After sonication they were centrifuged (30 min, 10 000 × *g*, 277 K). The supernatant was diluted to 2.5 mg protein/ml (final volume 200 ml) and passed over a column (2.5 × 10 cm) packed with amylose resin (New England Biolabs, #800-21 S, 15 ml, equilibrated with Tris-HCl buffer (120 ml as specified above). The protein solution was passed over the column at 1 ml per min. The column was washed with 150 ml Tris-HCl buffer (*vide supra*) and the fused protein (MBP/PdxH) eluted with the same buffer containing maltose (10 mM). The protein which eluted from 9 to 27 ml was yellow. The combined yellow protein fractions were concentrated by ultrafiltration ('8050'-cell, Amicon, Witten, Germany, with filter 'Omega Filter 10 K', Filtron) and the protein solution passed over a PD 10 Sephadex G 25 M matrix (Pharmacia, Freiburg, Germany).

2.5. Cleavage of the MBP / PdxH fusion protein

The MBP/PdxH fusion protein was cleaved using proteinase 'factor Xa' (New England Biolabs). Incubation was carried out at 277 K for 12 h with 5 units and 500 μg fused protein in 1 ml Tris-HCl buffer (*vide supra*). Again the protein was passed over the amylose column. PdxH eluted from 1 to 12 ml Tris-HCl buffer. The protein solution was concentrated (*vide supra*).

2.6. FPLC of PdxH or MBP / PdxH

The FPLC system consisted of a Pharmacia LKB gradient pump (2249) with a Pharmacia LKB Uvicord SII-Monitor (filter, 278 nm). Separation of proteins was carried out on an Ultra Pac TSK-6 3000 SW-FPLC Column (3135-300) of Pharmacia LKB, size 7.5 × 600 mm, filled with silica TP 5000, particle size 10 μm. Solvent system:

Fig. 2. Map
not to phage
to Lam and
P = *Pst*I, Pl

JUN-16-2003 MON 01:01 PM PIONEER HI BRED FAX NO. 2532184 P. 05

Notice: This material may be protected by copyright

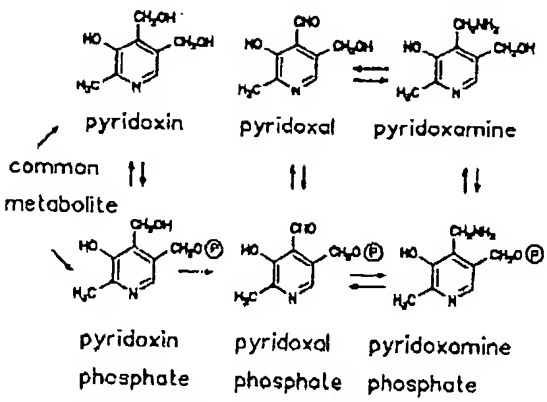

Fig. 1. Interconversion of B-6 vitamers in *E. coli*.

20 mM Tris-HCl (pH 7.4), 200 mM NaCl, 1 mM EDTA. Flow rate was 1 ml per min. The column was calibrated with: β-galactosidase (M_r 116400), phosphorylase B (M_r 96000), BSA (M_r 68000), ovalbumin (M_r 45000), carboanhydrase (M_r 30000).

2.7. Enzyme assay

Enzyme activity was determined using a phenylhydrazine method modified after Wada and Snell [10] with the following change: in order to measure steady state kinetic constants the incubation time was reduced to 10 minutes. Under these conditions measurements were in the linear range. The absorption of the hydrazone was measured in a spectrophotometer at 410 nm and the amount of hydrazone was calculated using a molar extinction coefficient of $\epsilon_{410} = 23000\ M^{-1}cm^{-1}$ [3].

All kinetic data are the mean of three independent experiments.

2.8. Mapping of *pdxH* to chromosomal position

The inserts on phages 13H4, 6F11 and 20B5 [1] were isolated by *Eco*RI cleavage and separation on agarose gel electrophoresis. The fragments were extracted from the gel and ligated into pUC19 linearized with the appropriate restriction enzyme. *E. coli* WG2 (*pdxH*$^-$) was transformed with the recombinant pUC19 plasmids.

3. Results

The gene product of *pdxH* is responsible for the oxidation of the 4′ carbon of B-6 vitamers to give the corresponding aldehyde (Fig. 1).

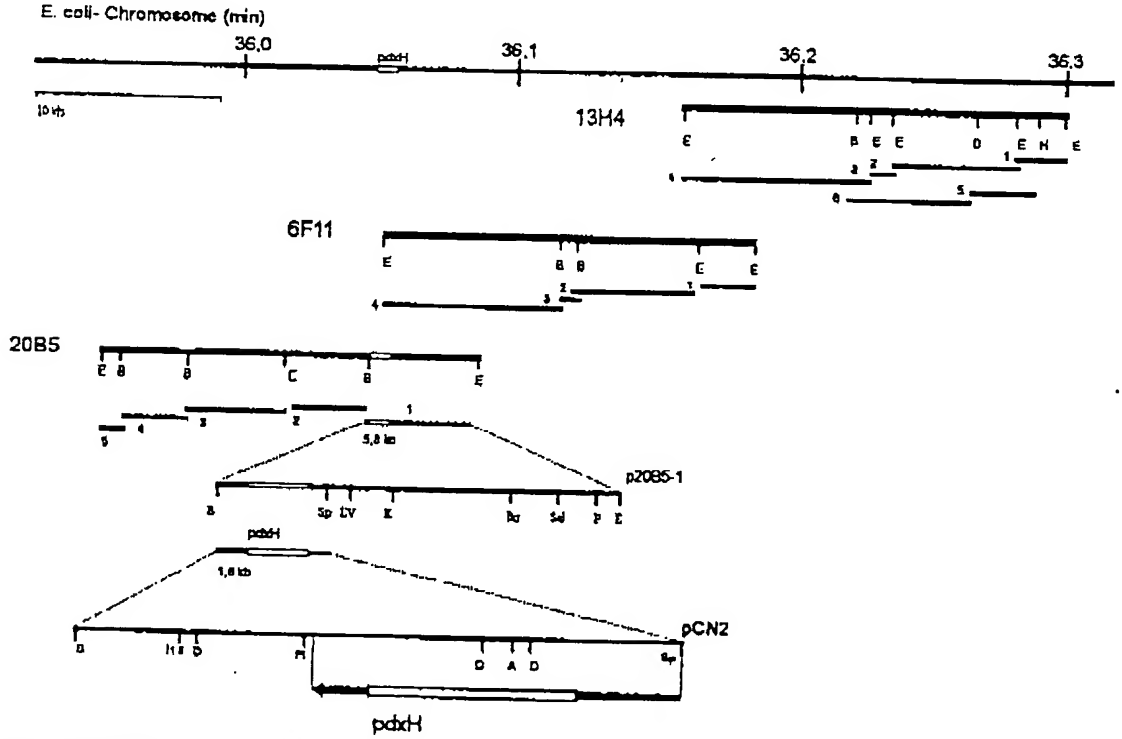

Fig. 2. Mapping of *pdxH* to chromosomal position, construction of plasmid pCN2 carrying the *pdxH* gene and assignment of the gene to phage 20B5 and not to phages 13H4 and 6F11 of Kohara et al. [1]. Location of *pdxH* on pCN2 is based on complementation of mutant WG2 (*pdxH*$^-$) and on comparison to Lam and Winkler's [12] published map. Restriction sites: E = *Eco*RI, B = *Bam*HI, H = *Hind*III, Sp = *Sph*I, EV = *Eco*RV, K = *Kpn*I, Bg = *Bgl*II, P = *Pst*I, Pl = *Pvu*I, Sal = *Sal*I, HII = *Hin*dII, D = *Dde*I, A = *Ava*II

JUN-16-2003 MON 01:02 PM PIONEER HI BRED FAX NO. 2532184 P. 06

Notice: This material may be protected by copyright.

Cotransduction experiments [13] located the *pdxII* gene to 36 min at the *E. coli* chromosome. This region of the chromosome is covered by the EMBL 4 phages 13H4, 6F11 and 20B5 (Fig. 2) of Kohara et al. [1]. Complementation studies with recombinant plasmids containing inserts of the above mentioned phages led to a plasmid named pCN2 derived from 20B5 (Fig. 2) which restored growth of the *E. coli* WG2 (*pdxH*$^-$) mutant. Plasmid pCN2 had the same pattern of restriction sites published for *pdxII* by Lam and Winkler [12]. These observation made it possible to precisely locate the *pdxII* gene to a stretch between 36.0 and 36.1 min of the *E. coli* chromosome corresponding to 1737 kilobases from the origin.

Using genomic DNA from *E. coli* and primers derived from the *pdxII* sequence published by Lam and Winkler [12] a *pdxII* gene was generated by PCR and ligated into the vector pMAL-c2 (New England Biolabs). This vector carries a gene (*malE*) which encodes a maltose binding protein (MBP) [17]. The *pdxII* gene and the *malE* gene were linked by a spacer encoding a cleavage site (Ile-Glu-Gly-Arg) for proteinase 'factor Xa'. After transformation the recombinant vector carrying *malE* and *pdxII* conferred growth to *E. coli* mutant WG2 (*pdxII*$^-$). This indicates that the MBP/PdxII fusion protein is physiologically active. Overexpression of the fused genes was induced by IPTG (isopropylthio-β-D-galactoside), protein was extracted from the cells and the MBP/PdxH fusion protein was purified to homogeneity by a one-step affinity chromatography on an amylose column. The homogeneous fusion protein was eluted by maltose. The protein is intensely yellow, as would be expected for a flavoprotein.

The activity of the fusion protein was determined by trapping the pyridoxal phosphate formed from either pyridoxol- or pyridoxamine phosphate as the hydrazone [10]. The hydrazone was quantitated photometrically. The enzyme accepted phosphorylated vitamers (pyridoxol phosphate, pyridoxamine phosphate) only, but no non-phosphorylated vitamers (pyridoxol or pyridoxamine). The pH optimum was broad (maximum at 7.7). The UV-spectrum of the intensely yellow MBP/PdxII fusion protein is shown in Fig. 3. Two maxima at 380 and 450 nm which disappear upon treatment with dithionite are typical of a protein containing flavine mononucleotide (FMN) [18]. When increasing amounts of FMN were added to the incubation mixture the velocity of the reaction and the final yield in pyridoxal phosphate increased (Table 1). This increase was not observed when FMN was replaced by flavine adenine dinucleotide (FAD).

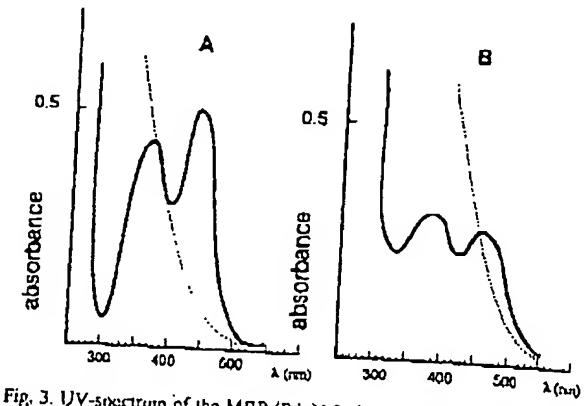

Fig. 3. UV-spectrum of the MBP/PdxII fusion protein (A) and UV-spectrum of authentic FMN (B) 20 μM each, in Tris-HCl buffer (pH 7.4) (*vide supra*). Solid line before, dotted line after reduction by dithionite. The UV-spectrum of the PdxH protein was essentially identical.

When the incubation mixture was flushed with nitrogen prior to incubation the activity of the enzyme dropped to 18% of the activity observed for an untreated incubation mixture. This indicates that oxygen is the electron acceptor in the oxidation process.

The enzyme is product inhibited as revealed by enzyme kinetic data with an inhibitor constant for pyridoxal phosphate of 8 μM. Lines in a reciprocal plot (Fig. 4) do not intersect on the $1/v$ axis but above the $1/s$ axis indicating that pyridoxal phosphate is not a competitive but a mixed type inhibitor.

When fusion protein was submitted to native PAGE, a weak and a strong protein band appeared. When repeated on SDS-PAGE only one band was visible. This indicated that part of the fusion protein was present as a dimer. Indeed gel exclusion chromatography showed a major and a minor protein fraction (Fig. 5A). Both protein fractions oxidized pyridoxol phosphate and had similar specific activities (2 nM/mg per s for the large protein, elution volume 8 to 10 ml; 1.9 nM/mg per s for the small protein, elution volume 14 to 20 ml).

Elution volume and cochromatography with a marker protein (M_r 45 000) were consistent with the assumption that the larger protein has a M_r of 137 000 (dimer) and the

Table 1
Influence of FMN on the activity of pyridoxol phosphate oxidase

Added FMN, final concentration (μM)	Pyridoxal phosphate formed (nmol, increase, %)	Velocity of reaction (nM/s per mg prot.)
0	70.2 (control)	3.34
0.2	73.2 (4)	3.48
2.0	76.2 (8.5)	3.62
6.0	81.0 (15.0)	3.80

Homogeneous MBP/PdxH fusion protein (50 μl of a solution of 700 μg protein in 1 ml buffer) and pyridoxol phosphate (10 μl of a solution of 100 μg in 1 ml buffer) were incubated (10 min 315 K) in buffer (20 mM Tris-HCl containing 200 mM NaCl, 1 mM) (EDTA, 1 mM NaN_3 and 1 mM dithiothreitol, pH 7.4).

JUN-16-2003 MON 01:02 PM PIONEER HI BRED FAX NO. 2532184 P. 07

Notice: This material may be protected by copyright

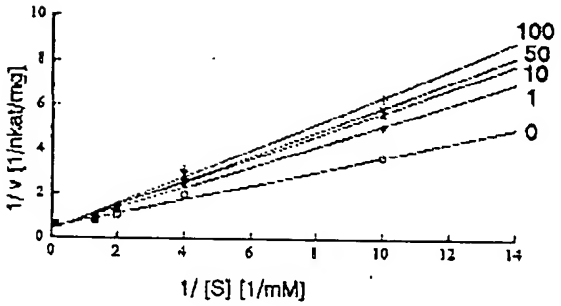

Fig. 4. Lineweaver–Burk plots of the enzymic oxidation (36.6 μg of homogeneous MBP/PdxH fusion protein in 1 ml buffer) of pyridoxol-5'-phosphate (μM) in the presence of increasing amounts (1, 10, 50, 100 μl of a 100 μM solution) of pyridoxal phosphate. Data are the mean of three independent experiments.

smaller protein a M_r of 68 500 (monomer). It was again concluded that a minor fraction of the fusion protein was present as a dimer.

The mixture of fusion proteins was now treated with proteinase 'factor Xa' to separate the PdxH protein (M_r 25 500) from the MBP domain (M_r 43 000). (The PdxH protein is unaffected by this process as it has no cleavage site for the proteinase). Size exclusion chromatography gave two fractions eluting with the expected volume (Fig. 5B). Both fractions were collected and their activity was determined.

If the PdxH protein forms a dimer (M_r 51 000) it should appear in a fraction larger than the MBP (M_r 43 000) (compare Fig. 5B). No protein, however, appeared with a molecular weight of M_r 51 000. In order to make sure that a M_r 51 000 protein would not be concealed in the fraction containing the MBP (M_r 43 000), this fraction was checked for pyridoxol phosphate oxidation.

No activity was found as opposed to the monomeric PdxH protein (M_r 25 500) (spec. act. 1.5 nM/mg per s) (Fig. 5B). Thus no indication was found that the PdxH protein dimerizes. Dimerisation observed in the protein preparations of the fusion protein (Fig. 5A) was therefore attributed to dimerisation of the MBP domain of the

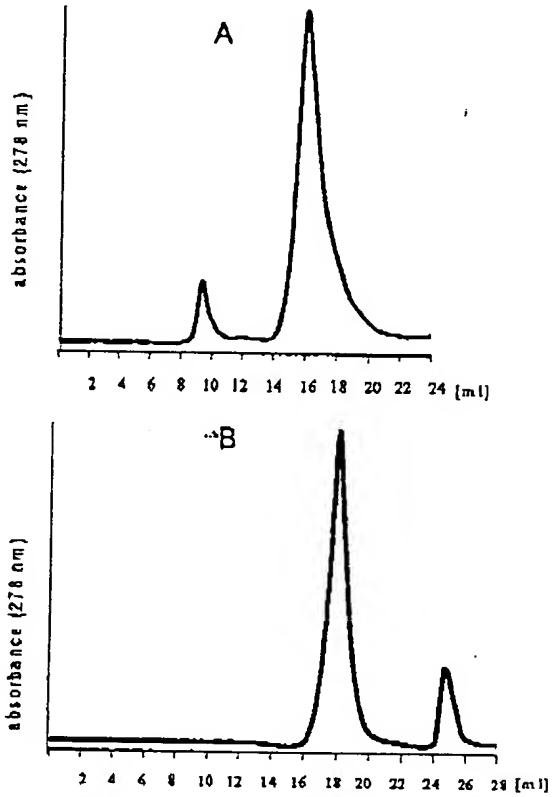

Fig. 5. FPLC chromatogram of the MBP/PdxH fusion protein after affinity chromatography on amylose resin (A) and of the PdxH protein after hydrolysis of the fusion protein by proteinase 'factor Xa' (B). Experimental details are given in Section 2. Numbers refer to ml effluent.

MBP/PdxH fusion protein. This is consistent with previous observations [19]. The monomeric PdxH protein was also separable from the MBP by affinity chromatography on the amylose column. While the MBP bound to the column, the PdxH protein eluted and was thus readily available for further characterization. The PdxH protein exhibits the same UV-spectrum as the fusion protein. Moreover, the K_m values for both the MBP/PdxH fusion

Table 2
Properties of MBP/PdxH fusion protein and PdxH protein (pyridoxol phosphate oxidase)

Property	MBP/PdxH fusion protein	PdxH (pyridoxol-5'-phosphate:oxygen oxidoreductase)
pH optimum	7.7	8.3
K_m (μM) (Pyridoxamine phosphate)	350	400
V_{max} (μkat/mg) (Pyridoxamine phosphate)	2	1.1
Turnover number (s^{-1})	137	28
K_M (μM) (Pyridoxol phosphate)	366	368
V_{max} (μkat/mg) (Pyridoxol phosphate)	5	1.3
Turnover number (s^{-1})	342	33

Calculation of the turnover number is based on *one* active site per monomer (M_r 68 500 or 25 500, respectively).

DEMCO

JUN-16-2003 MON 01:03 PM PIONEER HI BRED FAX NO. 2532184 P. 08

Notice: This material may be protected by copyright

protein and the PdxH protein are similar when both substrates (pyridoxol phosphate and pyridoxamine phosphate) are tested (Table 2).

However, also differences between the MBP/PdxH fusion protein and the PdxH protein were observed. The pH optimum of the PdxH protein was also broad but slightly higher (8.3 instead of 7.7; Table 2) when compared to the fusion protein. Moreover V_{max} and turnover number were significantly higher for the fusion protein. This is attributed to an improved stability of the fusion protein.

4. Discussion

Comparison of the *E. coli* pyridoxol-5′-phosphate:oxygen oxidoreductase (deaminating) (EC 1.4.3.5) with the corresponding enzymes from other sources shows that the enzymes share common features but are not identical in every respect. The molecular weight of the enzymes is within the same order of magnitude (M_r 25 000 to 30 000) in every case and the cofactor is FMN. Indeed the *E. coli* enzyme is intensely yellow in colour, exhibits a UV spectrum typical of FMN containing enzymes and its activity is oxygen dependent. While the enzymes isolated from animals form homodimers, no indication for a homodimer formation was found in the case of *E. coli*. Activity of the monomeric *E. coli* enzyme is clearly detectable. The enzymes from different sources are subject to product inhibition; the K_i for pyridoxal phosphate ranges from 1 to 5 μM depending on the pH and buffer [4].

The K_i for the *E. coli* enzyme is slightly higher (8 μM at pH 8.3). The enzyme from sheep brain is competitively inhibited [4], whereas our data indicate a mixed type inhibition for the *E. coli* enzyme.

Observations on the regulation of vitamin B-6 biosynthesis led Dempsey [20] to assume that the biosynthesis of B-6 vitamers in *E. coli* is "catalyzed by a series of sluggish enzymes" which are present in the range of normal enzyme concentrations. This implies that the enzymes of B-6 biosynthesis have a rather low turnover number and consequently a rather high K_m value (because only small amounts of B-6 vitamers are required). Indeed our data show in agreement with Dempsey's [20] assumptions that the K_m values determined for PdxH and the MBP/PdxH fusion protein are not particularly low (K_m 350 to 400 μM). This agrees very well with the kinetic data presented for the vitamin B-6 kinase from *E. coli* (K_m 300 μM for pyridoxal) [20].

Comparison of the maximum speed and turnover number of the PdxH protein and the MBP/PdxH fusion protein show that the fusion protein has a significantly higher maximum speed (v_{max}) (Table 2). This indicates that the MBP domain in the MBP/PdxH fusion protein stabilizes the PdxH protein. Instability of highly purified enzymes (in this case PdxH) is a common observation. The fact that both the MBP/PdxH fusion protein and the PdxH protein have similar K_m values shows that the MBP domain in the fusion protein does not affect the kinetic data of the pyridoxol phosphate oxidation process.

Our data suggest that the terminal step in the biosynthesis of pyridoxal phosphate in *E. coli* is the oxidation of pyridoxol phosphate. The fact that pyridoxamine phosphate is equally accepted as a substrate indicates that recycling of B-6 vitamers to pyridoxal phosphate is independent of transamination reactions that took place within a cell. Non-phosphorylated B-6 vitamers (pyridoxol, pyridoxamine) are not oxidized. This may indicate that phosphorylation occurs at an early step during the biosynthesis of pyridoxal phosphate (compare [21]).

In contrast, a vitamin B-6 kinase is also present in *E. coli* [22] indicating that pyridoxol or pyridoxal are the immediate metabolites derived from common primary precursors with the non-phosphorylated vitamers being subject to subsequent phosphorylation. This would be in agreement with the observation that a pyridoxal auxotrophic strain lacking pyridoxol phosphate oxidase accumulated both pyridoxol and pyridoxol-5′-phosphate when starved for pyridoxal [23].

The question of the terminal steps in pyridoxal phosphate biosynthesis, however, will not be settled before all observations are in agreement with data from genetic experiments indicating that pyridoxol phosphate oxidase (PdxH) is required under both aerobic and anaerobic growth conditions and that the presence of an alternative pathway or form of oxidase for pyridoxol oxidation in *E. coli* is likely [12]. We conclude that all available data are in agreement with a metabolic grid in which phosphorylated and non-phosphorylated B-6 vitamers are interconvertible as shown in Fig. 1.

Acknowledgements

The authors are grateful to Dr. Isono, Kobe, Japan for phages and to Dr. Faber, Bonn for sequencing the recombinant pMal-c2 plasmid. Supported by the 'Deutsche Forschungsgemeinschaft' and 'Fonds der Chemischen Industrie'.

References

[1] Kohara, Y., Akiyama, K. and Isono, K. (1987) Cell 50, 495–508.
[2] Kazarinoff, M.N. and McCormick, D.B. (1975) J. Biol. Chem. 250, 3436–3442.
[3] Merrill, A.H., Kazarinoff, M.N., Tsuge, H., Horiike, K. and McCormick, D.B. (1979) Methods Enzymol. 62, 568–574.
[4] Choi, S.Y., Churchich, J.E., Zaiden, E. and Kwok, F. (1987) J. Bacteriol. 262, 12013–12017.
[5] Clements, J.E. and Anderson, B.B. (1980) Biochim. Biophys. Acta 613, 401–409.

JUN-16-2003 MON 01:03 PM PIONEER HI BRED FAX NO. 2532184 P 09

Notice: This material may be protected by copyright

[6] Tsuge, H. and Okada, T. (1983) Biotechnol. Bioeng. 26, 412–418.
[7] Turner, J.M. and Happold, F.C. (1961) Biochem. J. 78, 364–372.
[8] Henderson, H.M. (1965) Biochem. J. 95, 775–779.
[9] Pflug, W. and Lingens, F. (1983) Hoppe-Seyler's Z. Physiol. Chem. 364, 1627–1630.
[10] Wada, H. and Snell, E.E. (1961) J. Biol. Chem. 236, 2089–2095.
[11] McCormick, D.B. and Merrill, A.H. (1980) in Vitamin B 6 — Metabolism and Role in Growth (Tryfiates, G.P., ed.), pp. 1–26, Food and Nutrition Press, Westport, CT.
[12] Lam, H.M. and Winkler, M.E. (1992) J. Bacteriol. 174, 6033–6045.
[13] Dempsey, W.B. (1969) J. Bacteriol. 97, 1403–1410.
[14] Tschopp, J. and Kirschner, K. (1980) Biochemistry 19, 4514–4521.
[15] Sambrook, J., Fritsch, E.F. and Maniatis, T. (1989) Molecular Cloning, A Laboratory Manual, 2nd Edn., Cold Spring Harbor Laboratory Press, Cold Spring Harbor, NY.
[16] Sanger, F., Nicklen, S. and Coulson, A. R. (1977) Proc. Natl. Acad. Sci. USA 74, 5463–5467.
[17] Guan, C., Li, P., Riggs, P.D. and Inouye, H. (1987) Gene 67, 21–30.
[18] Edmondson, D.E. and Singer, T.P. (1973) J. Biol. Chem. 248, 8144–8149.
[19] Duplay, P., Bedouelle, H., Fowler, A., Zabin, I., Saurin, W. and Hofnung, M. (1984) J. Biol. Chem. 259, 10606–10613.
[20] White, R. and Dempsey, W.B. (1970) Biochemistry 9, 4057–4064.
[21] Hill, R.E. and Spenser, I.D. (1986) in Coenzymes and Cofactors. Vitamin B-6 Pyridoxal Phosphate (Dolphin, D., Poulsen, R. and Avramovic, O., eds.), Vol. I, pp. 417–476, Wiley, New York.
[22] Dempsey, W.B. (1980) in Vitamin B 6 — Metabolism and Role in Growth (Tryfiates, G.P., ed.), pp. 93–111, Food and Nutrition Press, Westport, CT.
[23] Dempsey, W.B. (1966) J. Bacteriol. 92, 333–337.

JOURNAL OF BACTERIOLOGY, Oct. 1992, p. 6033–6045
0021-9193/92/196033-13$02.00/0
Copyright © 1992, American Society for Microbiology
Vol. 174, No. 19

Characterization of the Complex *pdxH-tyrS* Operon of *Escherichia coli* K-12 and Pleiotropic Phenotypes Caused by *pdxH* Insertion Mutations

HON-MING LAM AND MALCOLM E. WINKLER*

Department of Microbiology and Molecular Genetics, University of Texas Medical School, Houston, Texas 77030

Received 4 May 1992/Accepted 31 July 1992

We report the first molecular genetic analysis of a pyridoxine 5′-phosphate oxidase, the PdxH gene product of *Escherichia coli* K-12. Chromosomal insertions in and around *pdxH* were generated with various transposons, and the resulting phenotypes were characterized. The DNA sequence of *pdxH* was determined, and the promoters of *pdxH* and the downstream gene *tyrS*, which encodes tyrosyl-tRNA synthetase, were mapped by RNase T_2 protection assays of chromosomal transcripts. These combined approaches led to the following conclusions: (i) *pdxH* is transcribed from a sigma 70-type promoter and shares its transcript with *tyrS*; (ii) *tyrS* is additionally transcribed from a relatively strong, nonconventional internal promoter that may contain an upstream activating sequence but whose expression is unaffected by a *fis* mutation; (iii) PdxH oxidase is basic, has a molecular mass of 25,545 Da, and shares striking homology (>40% identity) with the developmentally regulated FprA protein of *Myxococcus xanthus*; (iv) mild pyridoxal 5′-phosphate limitation of *pdxH* mutants inhibits cell division and leads to formation of unsegregated nucleoids; (v) *E. coli* PdxH oxidase is required aerobically and anaerobically, but second-site suppressors that replace *pdxH* function entirely can be isolated; and (vi) *pdxH* mutants excrete significant amounts of L-glutamate and a compound, probably α-ketoisovalerate, that triggers L-valine inhibition of *E. coli* K-12 strains. These findings extend earlier observations that pyridoxal 5′-phosphate biosynthetic and aminoacyl-tRNA synthetase genes are often members of complex, multifunctional operons. Our results also show that loss of *pdxH* function seriously disrupts cellular metabolism in unanticipated ways.

Pyridoxal 5′-phosphate (PLP) and pyridoxamine 5′-phosphate (PMP) are important coenzymes that participate in many metabolic reactions, especially those involving amino acids (5, 22, 58). PLP and PMP are synthesized from pyridoxine (PN; vitamin B_6), pyridoxal (PL), and pyridoxamine (PM) by phosphorylation and oxidation reactions catalyzed by PN kinase (PN/PL/PM kinase; pyridoxal kinase; EC 2.7.1.35) and PNP oxidase (PNP/PMP oxidase; pyridoxaminephosphate oxidase; EC 1.4.3.5), respectively (Fig. 1) (15, 55). Of the three precursors, PN is thought to be the direct biosynthetic intermediate of PLP and is synthesized by bacteria, fungi, and higher plants (55). The biosynthesis of PN seems to occur by a branched pathway in *Escherichia coli* K-12 (33, 34) and most likely utilizes 4-hydroxythreonine (15, 33) and D-1-deoxyxylulose (23) as key intermediates. The last steps of PLP biosynthesis that take PN to PLP and PMP and interconvert the six B_6 vitamers (Fig. 1) seem to be present in all organisms (55).

The enzymology of eukaryotic PNP oxidase has been thoroughly studied in pig and sheep brain and rabbit liver (10, 11, 29, 36). Eukaryotic PNP oxidase is composed of two identical subunits (11, 29), and one flavin mononucleotide (FMN) molecule is bound to each dimer (11). Molecular oxygen is thought to be the sole electron acceptor in the oxidase reaction (29, 40). The oxidase seems to act preferentially on phosphorylated substrates (60) and is subject to product inhibition by PLP (Fig. 1) (60) that is reduced by partial proteolysis (30). Fluorescence polarization and resonance energy transfer studies suggest that there are protein-protein interactions between eukaryotic PNP oxidase and PN kinase (32).

Compared to the eukaryotic enzyme, relatively little has been reported about the biochemistry or genetics of prokaryotic PNP oxidase, which is encoded by *pdxH* at 36 min in the *E. coli* genetic map (15). Preliminary enzymological characterization in crude extracts suggested that *E. coli* PNP oxidase may be a flavoprotein that utilizes molecular oxygen as a substrate for at least 80% of its activity (56). However, interpretation of kinetic data was extremely difficult because of phosphatases in crude extracts which destroyed the PLP product. Point and MudI-8 insertion mutations in *pdxH* were isolated in both *E. coli* K-12 (25, 33) and *E. coli* B (14) strains by exploiting the property that *pdxH* mutants deficient in PNP oxidase grow on medium supplemented with PL but not with PN (Fig. 1). Recently, we reported the cloning of *E. coli* K-12 *pdxH*$^+$ (33). Complementation analysis of all known *pdxH* mutants demonstrated that *pdxH* consists of a single complementation group.

Here we report a structural analysis of the *pdxH* gene and its chromosomal transcription. Our data show that *pdxH*, like other *pdx* genes involved in PN biosynthesis (2, 17, 33, 34, 44, 54), forms a complex operon with a downstream gene, in this case, *tyrS*, which encodes the essential enzyme tyrosyl-tRNA synthetase (48). Physiological characterization of *pdxH* mutants revealed several unusual phenotypes, including a block in nucleoid segregation and cell division and excretion of L-glutamate (L-Glu) and a compound that inhibits L-isoleucine (L-Ile) biosynthesis. The absence of growth of *pdxH* insertion mutants aerobically and anaerobically, except when supplemented with PL, suggested that the PdxH enzyme is required for PLP biosynthesis in wild-

* Corresponding author. Electronic mail address: mwinkler@utmmg.med.uth.tmc.edu

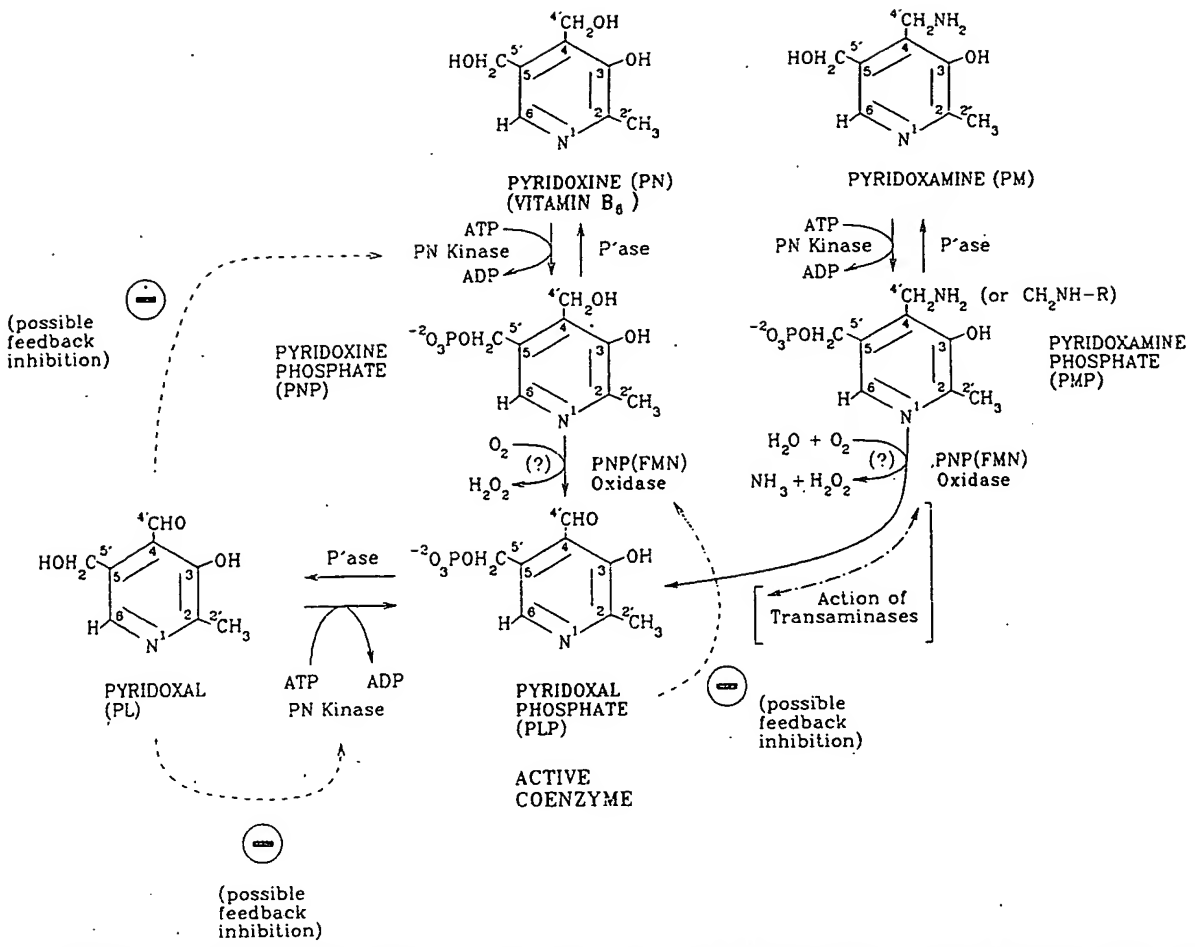

FIG. 1. Universal biosynthetic pathways leading from PN (vitamin B_6) to active PLP coenzyme and allowing interconversion of the six B_6 vitamers. The scheme is based on data reviewed in references 15 and 55. The minus signs indicate points of probable negative feedback inhibition of enzyme activities (36, 62). Alternative names for PN kinase (EC 2.7.1.35) and PNP oxidase (EC 1.4.3.5) include PN/PL/PM kinase, pyridoxal kinase, and PdxK kinase (in *E. coli*) and PNP/PMP oxidase, pyridoxaminephosphate oxidase, and PdxH oxidase (in *E. coli*), respectively.

type cells. However, isolation of suppressors that replace *pdxH* function suggests the presence of an alternative pathway or form of oxidase for PN oxidation in *E. coli*.

MATERIALS AND METHODS

Materials. The following enzymes and reagents were used in cloning, DNA sequencing, strain construction, and RNase T_2 transcript mapping experiments: restriction endonucleases, phosphorylated *Sph*I and *Bam*HI linkers, and M13 sequencing (−40) primer (New England Biolabs, Beverly, Mass., and Promega, Madison, Wis.); Riboprobe Gemini System II, restriction endonucleases, RQ1 DNase, and plasmid pGEM-3Z (Promega); RNase T_2 and bacterial alkaline phosphatase (Bethesda Research Laboratories, Gaithersburg, Md.); 17-mer oligonucleotide primers for DNA sequence determinations (Genosys, Inc., Woodlands, Tex.); T4 DNA polymerase (Boehringer Mannheim Biochemicals, Indianapolis, Ind.); pyrophosphatase and Sequenase (version 2.0) sequencing kits (United States Biochemical, Cleveland, Ohio); and Thermalbase sequencing kit (Stratagene, La Jolla, Calif.). Other chemicals used in these experiments included the following: radioactive compounds (Amersham Corp., Arlington Heights, Ill.); inorganic salts, organic solvents, BBL Gas-Pak supplies, and electrophoresis-grade agarose (Fisher Scientific, Fair Lawn, N.J.); acrylamide-bisacrylamide mixtures (29:1) (Curtin Matheson Scientific, Inc., Houston, Tex.); and ammonium persulfate and TEMED (*N,N,N',N'*-tetramethylethylenediamine) (Bio-Rad, Inc., Richmond, Calif.). Chemicals used for other experiments were DAPI (4',6-diamino-2-phenylindole); polylysine solution, antibiotics, and biochemicals (Sigma Chemical Co., St. Louis, Mo.); and glutamate dehydrogenase (Boehringer Mannheim Biochemicals). Ingredients for culture media included vitamin assay Casamino Acids, Bacto-Agar, yeast extract, and tryptone broth (Difco Laboratory, Detroit, Mich.).

Bacterial strains and plasmids. Bacterial strains, plasmids, and phages used in this study are listed in Table 1. P1 bacteriophage generalized transductions and 2-aminopurine mutagenesis of cells were carried out as described in reference 37. Recombinant plasmids were constructed by standard techniques (3, 46). Insertional mutagenesis of plasmids with mini-Mu*dII* elements was performed as previously described (9). Insertion positions in plasmids harboring mini-Mu*dII* elements were determined by restriction analy-

TABLE 1. Bacterial strains and plasmids

Strain or plasmid	Phenotype or genotype[a]	Source or reference
Strains		
DS941	*fis*::Km^r F$^-$ *ara-14 argE3 galK2 his-4 lacI^q lacZ*Δ*M15 leu-6 mtl-1 proA2 recF143 str-31 supE44 thi-1 thr-1 tsx-33 xyl-5*	J. Hinton collection
JC7623	*recB21 recC22 sbc-15 ara arg his leu pro thr*	A. J. Clark collection
NU816	W3110 Δ*lacU169 tna2 sup*^{0}	C. Yanofsky collection
NU887	SVS1100 *pdxH*::MudI-8-1	SVS1100 transposed with a MudI-8 element
NU901	SVS1100 *pdxA*::MudI-8	SVS1100 transposed with a MudI-8 element
NU908	SVS1100 *pdxH*::MudI-8-2	SVS1100 transposed with a MudI-8 element
NU1707	NU816 *pdxH*::MudI-8-1	NU816 × P1*kc*(NU887)
NU1708	NU816 *pdxH*::MudI-8-2	NU816 × P1*kc*(NU908)
NU1709	NU816 *pdxA*::MudI-8	NU816 × P1*kc*(NU901)
NU1730	NU1707(pNU216)	Transformant
NU1732	NU1708(pNU216)	Transformant
NU1735	NU1707(pNU217)	Transformant
NU1736	NU1708(pNU217)	Transformant
NU1737	JC7623 *zbe*::mini-MudII-3	JC7623 × linear pNU267
NU1738	JC7623 *zbe*::mini-MudII-2	JC7623 × linear pNU268
NU1739	JC7623 *zbe*::mini-MudII-1	JC7623 × linear pNU269
NU1740	JC7623 *zbe*::mini-MudII-4	JC7623 × linear pNU270
NU1814	NU816(pNU216)	Transformant
NU1815	NU816(pNU217)	Transformant
NU1833	NU816 *zbe*::mini-MudII-3	NU816 × P1*kc*(NU1737)
NU1835	NU816 *zbe*::mini-MudII-2	NU816 × P1*kc*(NU1738)
NU1837	NU816 *zbe*::mini-MudII-1	NU816 × P1*kc*(NU1739)
NU1839	NU816 *zbe*::mini-MudII-4	NU816 × P1*kc*(NU1740)
SVS1100	*bglR551* Δ(*lac-argF*)*U169*	V. Stewart collection
TT6547	*supD ara-14 eda-50* Δ*lacU169 metF*(Am) *mtl-1 rpsL136 thi-1 tonA31 tsx-78 xyl-5*	J. Roth (26)
TT9894	TR6547 Muc62ts MudI-8 dilysogen	J. Roth (26)
TX2268	NU816(pTX281)	Transformant
TX2277	NU1707(pTX281)	Transformant
TX2278	NU1708(pTX281)	Transformant
TX2351	NU816(pBR325)	Transformant
TX2361	JC7623 ORF1::Km^r(*Sph*I)>	JC7623 × linear pTX294
TX2362	JC7623 ORF1::<Km^r(*Sph*I)	JC7623 × linear pTX295
TX2363	NU816 ORF1::Km^r(*Sph*I)>	NU816 × P1*vir*(TX2361)
TX2364	NU816 ORF1::<Km^r(*Sph*I)	NU816 × P1*vir*(TX2362)
TX2451	NU816 *fis*::Km^r	NU816 × P1*vir*(DS941)
Plasmids		
pBR325	ColE1 replicon; Ap^r Tc^r Cm^r	Lab stock (8)
pGEM-3Z	Vector for riboprobe synthesis; Ap^r	Promega
pMB2190	Km^r in pBR327 derivative; Ap^r Tc^r	B. Nichols collection
pNU216	ORF1-*pdxH*$^+$ cloned in pBR325; Ap^r Cm^r	Lab stock (33)
pNU217	*pdxH*$^+$-*tyrS*$^+$ cloned in pBR325; Ap^r Cm^r	Lab stock (33)
pNU267	pNU217 (*zbe*::mini-MudII-1); *pdxH*$^+$; Ap^r Cm^r	This work
pNU268	pNU217 (*zbe*::mini-MudII-2); *pdxH*$^+$; Ap^r Cm^r	This work
pNU269	pNU217 (*zbe*::mini-MudII-3); *pdxH*$^+$; Ap^r Cm^r	This work
pNU270	pNU217 (*zbe*::mini-MudII-4); *pdxH*$^+$; Ap^r Cm^r	This work
pTX281	pBR325 containing a 1.8-kb *Sph*I-*Bam*HI fragment from pNU217; *pdxH*$^+$; Ap^r Cm^r	This work
pTX292	pBR325 lacking *Sph*I site	This work
pTX293	pTX292 containing a 5.4-kb *Bam*HI-*Bam*HI fragment from pNU216 *pdxH*$^+$; Ap^r Cm^r	This work
pTX294	pTX293 ORF1::Km^r(*Sph*I)> *pdxH*$^+$; Ap^r Cm^r	This work
pTX295	pTX293 ORF1::<Km^r(*Sph*I) *pdxH*$^+$; Ap^r Cm^r	This work
pTX303	0.57-kb *Ava*I-*Sac*II fragment from pTX281 cloned into the *Bam*HI site of pGEM-3Z; *pdxH* transcription same orientation as *lacZ*; Ap^r	This work
pTX306	0.76-kb *Sac*II-*Sph*I fragment from pTX281 cloned into the *Bam*HI site of pGEM-3Z; *pdxH* transcription same orientation as *lacZ*; Ap^r	This work

[a] < or > indicates that the direction of transcription of *kan* in the Km^r cassette is opposite to or the same as that of *pdxH*, respectively. Km^r(*Sph*I) signifies the presence of a kanamycin resistance cassette cloned into the *Sph*I site of ORF1 (Fig. 2). mini-MudII-1-4 mapped immediately downstream from *tyrS* (Fig. 2). The mini-MudII-2 element in NU1835 (Fig. 2) was in the opposite orientation as *tyrS* but formed an active *lacZ* gene fusion. Ap^r, ampicillin resistant; Cm^r, chloramphenicol resistant; Tc^r, tetracycline resistant.

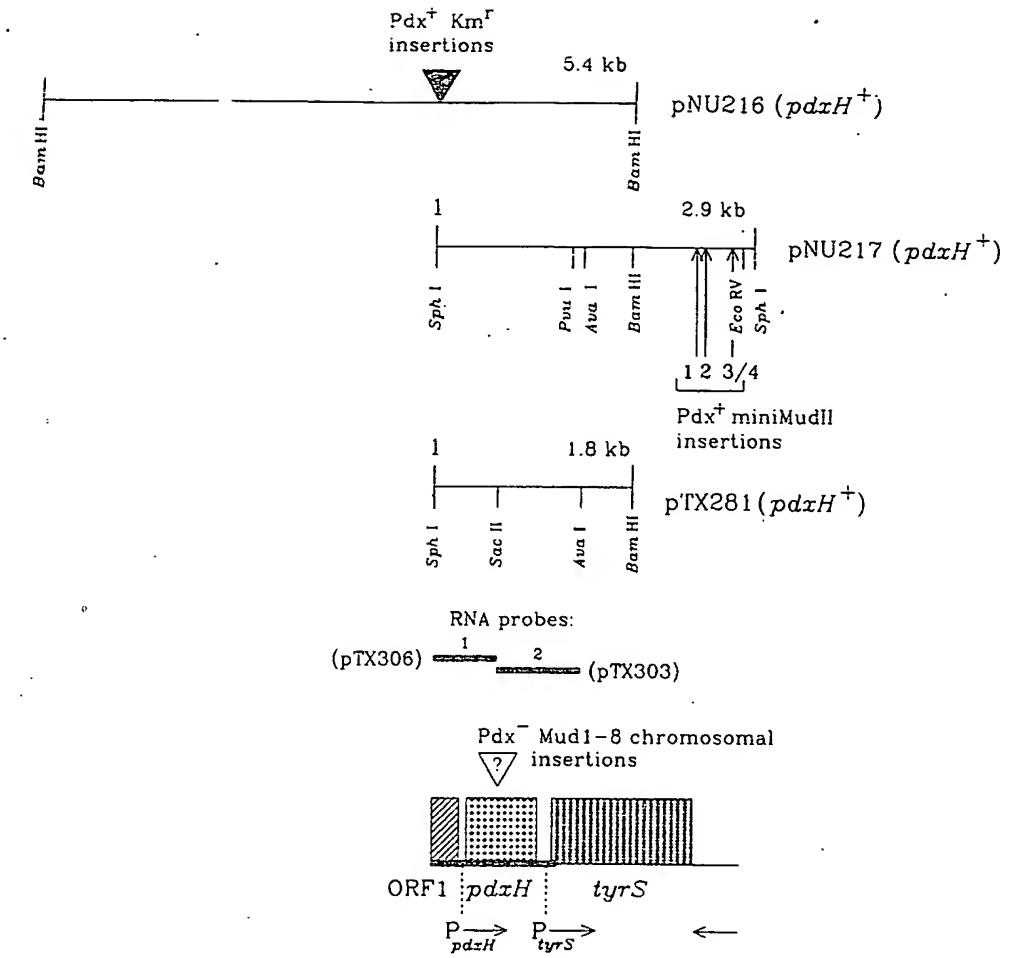

FIG. 2. *pdxH*$^+$ recombinant plasmids and locations of insertion mutations in and around *pdxH* in recombinant plasmids and the *E. coli* K-12 chromosome. The whole figure is drawn to scale. *pdxH*::Mu*d*I-8, ORF1::Km^r, and *zbe*::mini-Mu*d*II insertions were isolated or constructed and crossed into the bacterial chromosome as described in Materials and Methods. Exact positions of Mu*d*I-8 elements within *pdxH* are unknown. Restriction mapping showed that the *zbe*::mini-Mu*d*II elements were extremely close to the end of *tyrS*. *zbe*::mini-Mu*d*II-2 formed active *lacZ* gene fusions but was in the opposite orientation to *tyrS*. The positions of the two RNA probes used to map in vivo transcripts are indicated. The dark black line in the summary diagram at the bottom marks the new DNA sequence reported in Fig. 3. The positions and identities of the reading frames and promoters are based on data presented here and in reference 4 for the *tyrS* coding region. No transcription was detected in vivo from either DNA strand in the 280-bp region upstream from *pdxH* (ORF1; see text).

ses. Kanamycin resistance cassettes with *Sph*I linkers at their ends were cloned in both orientations into the *Sph*I site in pTX293 to disrupt the open reading frame upstream from *pdxH* (ORF1, Fig. 2). Insertions imparting antibiotic resistances were crossed from linearized plasmids into the chromosome of *recBC sbc* mutant JC7623 as detailed before (1, 63) *pdxH*::Mu*d*I-8 chromosomal mutants and plasmids pNU216 and pNU217 were isolated previously in this laboratory (33). Plasmid pTX281 (Fig. 2) was constructed by subcloning the 1.8-kb *Sph*I-*Bam*HI fragment from pNU217 into pBR325. Plasmids pTX303 and pTX306, which were used for RNase T_2 protection assays, were constructed by ligating *Bam*HI linkers onto the 0.57-kb *Ava*I-*Sac*II and 0.76-kb *Sac*II-*Sph*I fragments from pTX281, respectively, and cloning the resulting fragments into the *Bam*HI site of vector pGEM-3Z.

Culture conditions. LBC rich medium was Luria-Bertani broth supplemented with 30 μg of L-cysteine per ml. Minimal Vogel-Bonner (1XE) medium containing 0.01 mM $FeSO_4$ was prepared as described in reference 13. MMG was 1XE salts plus 0.4% (wt/vol) glucose. Where specified, MMG was supplemented with 0.5% (wt/vol) vitamin assay Casamino Acids. PL was added to media at a final concentration of 1 μM. Other growth conditions are described in the figure legends and table footnotes.

DNA sequence analysis. DNA sequences were determined by the Sequenase and Thermalbase variations of the Sanger dideoxynucleotide method from single-strand mp18 and mp19 M13 phage clones (47) as described previously (44, 49). Both strands were sequenced with each enzyme or by using at least two different reaction mixtures containing dGTP, dITP, or deaza-dGTP according to the manufacturer's instructions. Synthetic primers were used to sequence along the M13 phage clones and to close all gaps. DNA sequences were analyzed with the University of Wisconsin Genetics Computer Group and PCGene (Intelligenetics, Inc., Moun-

tain View, Calif.) computer programs, which included access to the GenBank, EMBL, and Ecoseq (45) data bases.

RNase T_2 transcript analysis. RNase T_2 mapping of in vivo transcripts was performed as described previously (49) with the following changes: (i) total cellular RNA was prepared by a boiling lysis method in which cells were lysed directly in culture medium without centrifugation (18); (ii) the last step of the RNA purification included treatment with RQ1 (RNase-free) DNase (49); (iii) RNase T_2 digestion was carried out at 37°C for at least 4 h, instead of at 30°C; and (iv) after digestion with RNase T_2, samples were extracted with phenol-chloroform-isoamyl alcohol (24:23:1 by vol) and precipitated with 2 volumes of ethanol. After electrophoresis, gels were dried, and radioactive bands were quantitated with a beta scope (Betagen Corp., Waltham, Mass.).

Light microscopy, amino acid analyses, and L-glutamate bioassays. Cell morphologies were examined following DAPI staining using combined phase-contrast and fluorescence light microscopy as described in reference 24. Amino acid analyses were performed by the Analytical Chemistry Center of this university by using ion-exchange high-performance liquid chromatography (HPLC) provided as part of an automated Pharmacia-LKB system. Bioassay of L-glutamate by glutamate dehydrogenase activity was performed as described in reference 6.

Nucleotide sequence accession number. The GenBank accession number for the sequence in this paper is M92351.

RESULTS

Localization of *pdxH* by subcloning and insertion mutagenesis. We reported previously the isolation of *pdxH*::MudI-8 insertion mutants and two overlapping clones, pNU216 and pNU217, that complemented *pdxH* insertion and point mutations (Fig. 2) (33). We isolated one smaller subclone of pNU217 that still complemented *pdxH* mutants (pTX281, Fig. 2). DNA sequence analysis presented below conclusively demonstrated that plasmid pTX281 contained only one intact open reading frame that must correspond to the *pdxH*$^+$ gene (Fig. 2 and 3). Besides *pdxH*$^+$, pTX281 contained part of an upstream open reading frame (ORF1) and the first half of downstream *tyrS*, whose DNA sequence was reported previously (Fig. 2 and 3) (4).

Insertion mutagenesis confirmed the placement of *pdxH*$^+$ between ORF1 and *tyrS*. We introduced kanamycin resistance (Km^r) cassettes in both orientations into the *Sph*I site of plasmid pNU216 to disrupt ORF1 (Fig. 2). Insertions close to the end of *tyrS* were generated by transposition of mini-MudII(Km^r) elements into pNU217 (Fig. 2). The kanamycin resistance cassettes and mini-MudII insertion mutations were crossed into the bacterial chromosome via homologous recombination from linearized plasmid DNA (1, 63). All *pdxH*::MudI-8, ORF1::Km^r, and mini-MudII insertions were transduced into strain NU816 (W3110 Δ*lac*). The resulting strains were checked and found to lack plasmids, which is consistent with recombination of insertion elements into the bacterial chromosome.

Chromosomal *pdxH*::MudI-8 mutations caused a requirement for exogenous PL that could not be satisfied by PN (33). By contrast, chromosomal insertions in ORF1 upstream from *pdxH* or downstream from the end of *tyrS* did not show observable growth defects in LBC medium or MMG. These observations confirmed that ORF1 is not required for *pdxH* function. Strong polar effects of ORF1 or *pdxH* insertions on *pdxH* or *tyrS* expression would result in a PL requirement or impaired growth, respectively. Such strong polar effects were not observed, which suggested that *pdxH* and *tyrS* probably are expressed independently, at least under the growth conditions tested. The latter conclusion was confirmed by the transcription analysis presented below. Finally, one of the chromosomal mini-MudII insertions located downstream near the end of *tyrS* (NU1835, *zbe*::mini-MudII-2, Table 1; Fig. 2) formed an active *lacZ* gene fusion, as judged by deep red colony color on MacConkey-lactose plates. This gene fusion was in the opposite orientation to *pdxH* and *tyrS* (Fig. 2), consistent with transcription in the opposite direction to *pdxH* and *tyrS*.

DNA sequence analysis of *pdxH*. DNA sequence analysis delineated the genetic organization of *pdxH* and adjacent loci (Fig. 3). The open reading frame between nucleotides (nt) 310 and 966 was identified as the *pdxH* gene product on the basis of the genetic criteria described above. The translation start was assigned on the basis of the strong homology described below between *E. coli pdxH* and *Myxococcus xanthus fprA*. AUG at nt 310 is the only possible translation start that can accommodate this homology. The *pdxH* translation start contains a relatively poor match (three of six) to the Shine-Dalgarno ribosome-binding sequence (Fig. 3). Predicted properties of *E. coli* PdxH protein and comparisons with the eukaryotic enzyme are in the Discussion.

FASTA and TFASTA searches of EMBL-GenBank revealed a remarkable homology between *E. coli* PdxH and *M. xanthus* FrpA (Fig. 4) (20). Degrees of identity and overall similarity are about 43 and 64%, respectively, over the entire length of both polypeptides (Fig. 4). The *fprA* gene seems to be developmentally regulated in *M. xanthus* (20); however, no function was discovered for the FprA protein other than its ability to bind FMN tightly but not covalently (50). FMN binding is a property expected for PNP oxidase from enzymological characterizations of the purified eukaryotic enzyme (11) and activities in crude extracts of *E. coli* (see the introduction) (56). Together, the homology with the *E. coli* PdxH protein and its high affinity for FMN strongly suggest that *fprA* encodes PNP oxidase in *M. xanthus*. Possible ramifications of the developmental control of *fprA* to PLP biosynthesis are considered in the Discussion.

The unknown open reading frame immediately upstream from *pdxH* (ORF1; Fig. 2 and 3) matched a partial open reading frame of unknown function from *Yersinia enterocolitica* (ORF4'; GenBank accession X60449). However, chromosomal insertions in ORF1 failed to show discernible phenotypes (Fig. 2), and no chromosomal transcription from the ORF1 region was detected from either DNA strand in cells growing exponentially in LBC medium (see below). Consequently, we do not presently know the function, if any, of the 250 bp preceding the *pdxH* promoter (marked in Fig. 3; see below). In contrast, the open reading frame immediately downstream from the end of *pdxH* was readily identified as the essential *tyrS* gene, which encodes tyrosyl-tRNA synthetase (Fig. 2 and 3) (4). We demonstrate a relationship between *pdxH* and *tyrS* transcription in the next section.

Transcript mapping of *pdxH* and *tyrS* promoters. The close proximity of *pdxH* and *tyrS* prompted us to examine whether *pdxH* and *tyrS* share a transcript and constitute a complex operon. RNA probes 1 and 2 (Fig. 2) were synthesized corresponding to the ORF1-*pdxH* and *pdxH-tyrS* junctions, respectively, from both DNA strands as described in Materials and Methods. Total cellular RNA was purified from strain NU816 growing exponentially in LBC medium at 37°C with shaking and hybridized to the four RNA probes. Figure 5 shows the segments of the probes protected from RNase T_2

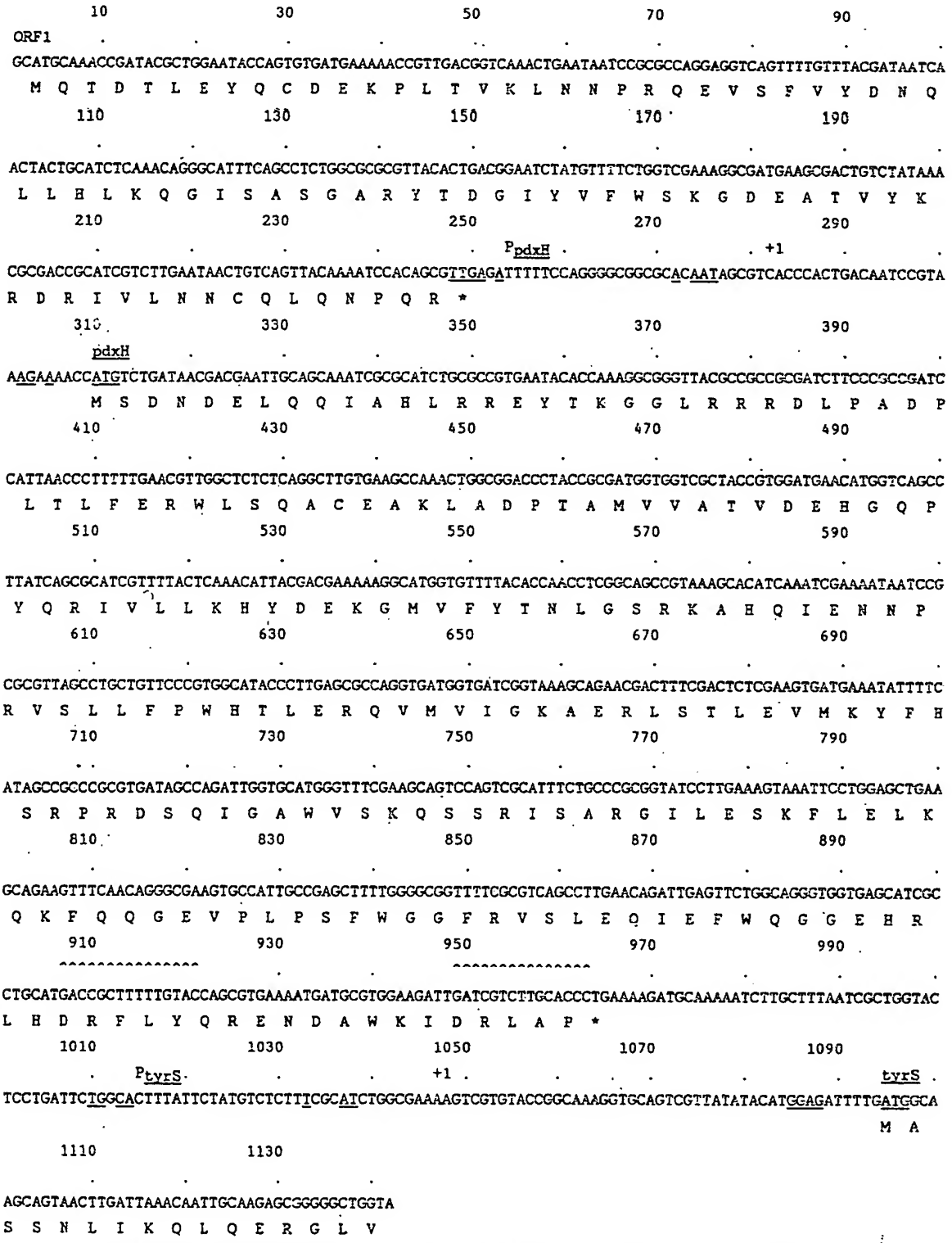

FIG. 3. DNA sequence of *pdxH* extending to the start of *tyrS*. The sequence is numbered from the *Sph*I site at the left end of the chromosomal insert in *pdxH*$^+$ recombinant clones pNU217 and pTX281 (Fig. 2). Probable transcription starts are indicated by +1. Likely σ-70 promoter consensus sequences, ribosome binding sites, and translation start codons are underlined. Two putative Fis protein binding sites are marked (*) in the A-T-rich region immediately upstream of P_{tyrS}. Transcript mapping experiments indicated that no transcription termination appears to occur between *pdxH* and *tyrS* (see Fig. 5 and 6). Other features of the DNA sequence are described in the text.

```
PdxH    7 LQQIAHLRREYTKGG.........LRRRDLPADPLTLFERWLSQACEAKLA 48
          :. :. :. | |  .          |:|  :|:||:  |. ::..| :|  .
FprA    1 MRTLTCVPDESTAKVHTCRAPFMLHRVNIPPDPIQRFAELFERAKQAIAV 50

         49 DPTAMVVATVDEHGQPYQRIVLLKHYDEKGMVFYTNLGSRKAHQIENNPR 98
            ||.|||||||::.|.| .|:|||||.:|.:|:|||||  :|||:::  .:|
         51 DPNAMVVATVGDDGRPSARVVLLKDFDARGFVFYTNHESRKGREARAHPY 100

         99 VSLLFPWHTLERQVMVIGKAERLSTLEVMKYFHSRPRDSQIGAWVSKQSS 148
            ..| | |:.|: ||.| |:.||:.. |.  ||:||:|:|||:|||.| ||
        101 AALCFYWQPLNEQVRVEGRVERVTDAEADAYFQSRARGSQVGAWASLQSQ 150

        149 RISARGILESKFLELKQKFQQGEVPLPSFWGGFRVSLEQIEFWQGGEHRL 198
            .:..|: ||.:. |:.||:....|| |. |:|||  :.||||::.| ||
        151 PLATREELEARVAEVEQKYAGQPVPRPPHWSGFRVVPDRIEFWHAQESRL 200

        199 HDRFLYQRENDAWKIDRLAP 218
            ||| :| ||:::|:.:.| |
        201 HDRHVYLREDGGWRTQMLYP 220
```

FIG. 4. Amino acid alignment between the *E. coli pdxH* gene product, PNP oxidase, and the *M. xanthus fprA* gene product, which is known to bind FMN. The *M. xanthus* sequence was reported by Hagen and Shimkets (20). The homology between PdxH and FprA was originally discovered in a FASTA search of EMBL-GenBank (initial alignment score = 475). The alignment in the figure was generated with the Bestfit program in the University of Wisconsin Genetics Computer Group software package. Degrees of identity and overall similarity are about 43 and 64%, respectively, over the entire length of both polypeptides. No obvious putative FMN and flavin adenine dinucleotide (41, 53), ferredoxin (64), or NAD (7) binding site motifs were detected in either enzyme. Likewise, a lysine-containing peptide similar to the one that reacts with bis-PLP in sheep brain (10) was not found in either protein. Relationships between amino acid pairs: |, identical; :, highly conserved; ., moderately conserved.

digestion. Undigested probes are in the odd-numbered lanes, and positions of additional RNA size standards are indicated. Hybridization of probe 1 corresponding to the *pdxH* noncoding strand showed one strong band with a size of 491 ± 5 nt (Fig. 5, lane 4). We interpret this band to represent transcription from a promoter immediately upstream from the translation start of *pdxH* (P_{pdxH}, Fig. 2 and 3). The most likely placement of P_{pdxH} indicates an almost perfect −35 σ-70 consensus region and a −10 region containing the most highly conserved A and T bases (Fig. 3). One somewhat unusual feature of P_{pdxH} is the runs of T and G residues between the −35 and −10 regions.

No transcription from the ORF1 region was detected with probe 1 *pdxH* noncoding or opposite strand (Fig. 5, lanes 4 and 2, respectively). In some experiments, gels were run so that even short protected fragments should have been detectable (data not shown). We interpret the faint band below the strong band in Fig. 5, lane 4, to represent a fragment corresponding to transcription from P_{pdxH} which was formed by slight overdigestion by RNase T_2. Its relatively large size (≈480 nt) makes it unlikely that this fragment corresponds to ORF1 transcription on the same DNA strand as *pdxH*. The absence of any transcription from the probe 1 *pdxH* coding strand (Fig. 2, lane 2) also demonstrated that our total RNA preparations lacked detectable DNA contamination.

Hybridization with probe 2 *pdxH-tyrS* noncoding strand showed two protected fragments of 573 ± 5 and 294 ± 5 nt (Fig. 5, lane 8). The 573-nt fragment represents full-length protection of *pdxH-tyrS* chromosomal probe 2 sequences by mRNA, where the difference in size with the undigested probe (lane 7) is due to plasmid linker sequences. Thus, there is contiguous transcription between *pdxH* and *tyrS*. Again, the coding strand control showed no transcription and no DNA contamination that could account for full-length protection of the noncoding strand probe (Fig. 5, lane 6). The molar amount of the 491-plus-480-nt P_{pdxH} transcript (lane 4) equaled that of the 573-nt *pdxH-tyrS* transcript within less than 10% experimental error (lane 8). This observation suggests that all of the *pdxH-tyrS* transcript arose from transcription initiation at P_{pdxH}.

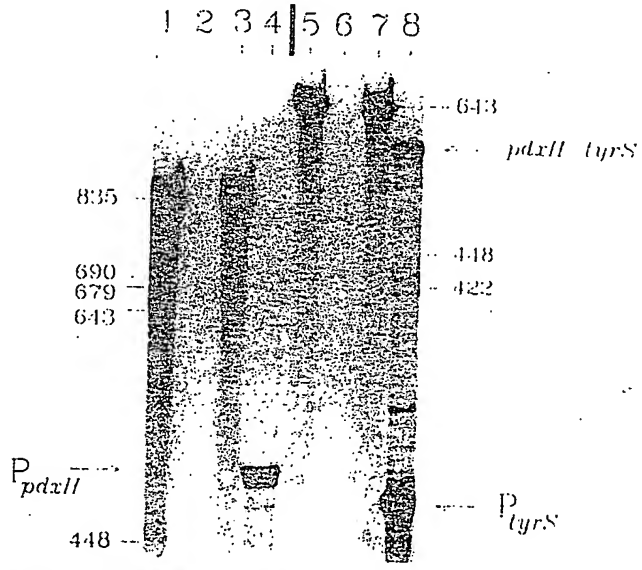

FIG. 5. RNase T_2 mapping of chromosomal transcription at the beginning o *pdxH* and from the *pdxH-tyrS* junction. Total RNA was prepared from *pdxH*$^+$ strain NU816 grown in LBC medium at 37°C with shaking as described in Materials and Methods. RNA probes 1 and 2 corresponding to the ORF1-*pdxH* and *pdxH-tyrS* junctions, respectively (Fig. 2), were synthesized from both DNA strands, and RNase T_2 protection assays of chromosomal transcripts were performed as detailed in Materials and Methods. Numbers indicate positions of RNA size standards. Lanes 1 to 4 and 5 to 8 were loaded onto the same gel at different times, which is why the standard positions are different on the two sides of the gels. Protected probe fragments corresponding to transcription initiation at the P_{pdxH} (491 ± 5 nt) and internal P_{tyrS} (295 ± 5 nt) promoters and the contiguous *pdxH-tyrS* transcript (573 ± 5 nt) are indicated. Odd-numbered or even-numbered lanes contain unhybridized RNA probes or RNA probes hybridized with total RNA, respectively. Lanes 1 and 2, probe 1 *pdxH* coding strand (i.e., probe sequence is the same as *pdxH* mRNA); lanes 3 and 4, probe 1 *pdxH* noncoding strand (i.e., probe sequence is complementary to *pdxH* mRNA); lanes 5 and 6, probe 2 *pdxH-tyrS* coding strand; lanes 7 and 8, probe 2 *pdxH-tyrS* noncoding strand.

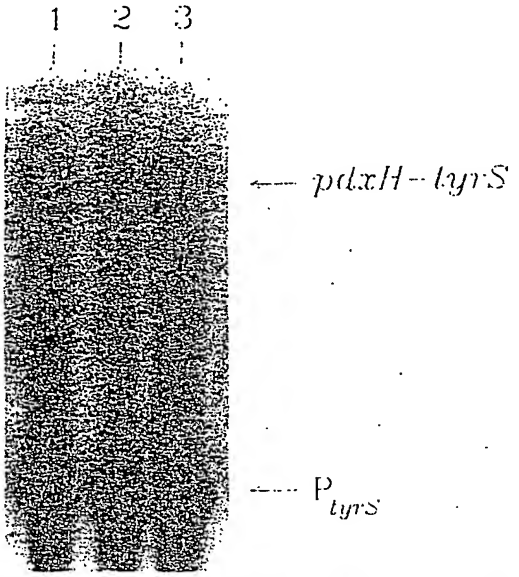

FIG. 6. Transcript analysis of *pdxH*::Mud*I*-8 and *fis*::Km^r mutants. Total RNA was prepared from *pdxH*$^+$ parent NU816 (lane 1), *pdxH*::Mud*I*-8 mutant NU1708 (lane 2), and *pdxH*$^+$ *fis*::Km^r mutant TX2451 (lane 3). TX2451 was grown in LBC medium, and NU816 and NU1708 were grown in LBC-PL medium with shaking at 37°C. Purification of RNA and RNase T_2 protection assays of chromosomal transcripts were performed as described for Fig. 5 and in Materials and Methods. RNA probe 2 (Fig. 2) corresponding to the *pdxH-tyrS* noncoding strand was used in each experiment. Protected probe fragments corresponding to the contiguous *pdxH-tyrS* transcript and to transcription initiation at the internal P_{tyrS} promoter are indicated (Fig. 5, lanes 7 and 8).

TABLE 2. Effect of *pdxH*::Mud*I*-8 mutations and *pdxH*$^+$ clones on aerobic and anaerobic growth[a]

Strain(s)	Colony growth[b] on:							
	LBC medium		LBC medium-PL		MMG-CAA		MMG-CAA-PL	
	$+O_2$	$-O_2$	$+O_2$	$-O_2$	$+O_2$	$-O_2$	$+O_2$	$-O_2$
pdxH$^+$ parent (NU816)	+	+	+	+	+	+	+	+
pdxH$^+$ parent with recombinant plasmid:								
pNU216 (NU1814)	+	+	+	+	+	−	+	−
pNU217 (NU1815)	+	+	+	+	+	sm	+	sm
pTX281 (TX2268)	+	+	+	+	+	sm	+	sm
pdxH::Mud*I*-8 mutants (NU1707, NU1708)	sm	sm	+	+	−	−	+	+
pdxH::Mud*I*-8 mutants with recombinant plasmid:								
pNU216 (NU1730, NU1732)	+	+	+	+	+	−	+	−
pNU217 (NU1735, NU1736)	+	+	+	+	+	sm	+	sm
pTX281 (TX2277, TX2278)	+	+	+	+	+	sm	+	sm

[a] Fresh patches of each strain were made by streaking dimethyl sulfoxide-stored permanent cultures onto LBC medium (NU816), LBC medium–PL–50 μg of ampicillin per ml (*pdxH*::Mud*I*-8 strains), or LBC medium–25 μg of chloramphenicol per ml (strains containing recombinant plasmids) plates that were incubated aerobically at 37°C overnight. Cells were then streaked from the fresh patches onto the plates indicated, which lacked antibiotic. Plates were incubated at 37°C aerobically ($+O_2$) or anaerobically ($-O_2$) in a BBL GasPak System containing an indicator strip. The same results were obtained for cells streaked onto plates containing G medium supplemented with glycerol and nitrate (52) (data not shown). Cells streaked onto control plates containing E medium supplemented with glycerol but lacking nitrate failed to grow anaerobically.

[b] +, normal-sized colonies; sm, small colonies; −, no growth. Larger colonies of strains originally containing *pdxH*$^+$ clones that arose on MMG were found to have lost the recombinant plasmids. CAA, Casamino Acids.

The 294-nt protected fragment of probe 2 (Fig. 5, lane 8) corresponds to independent transcription initiation from a relatively strong internal promoter (P_{tyrS}, Fig. 2, and 3). To prove that this band represents transcription from an internal promoter, we prepared total mRNA from a *pdxH*::Mud*I*-8 insertion mutant and repeated the RNase T_2 protection assay (Fig. 6, lanes 1 and 2). In this context, the *pdxH*::Mud*I*-8 insertion was completely polar and obliterated the *pdxH-tyrS* band (Fig. 6, lane 2). However, the amount of the 294-nt P_{tyrS} band was unaffected by the insertion mutation within 10% error, consistent with independent transcription initiation rather than mRNA processing. Quantitation of gel bands on a beta scope indicated that about 20% of *tyrS* steady-state transcripts originated at P_{pdxH} and 80% originated at P_{tyrS} in bacteria growing exponentially in LBC medium at 37°C. In support of this interpretation, the chemical half-lives of the *pdxH-tyrS* and P_{tyrS} transcripts were approximately the same (≈1 min) under these culture conditions following addition of 0.5 mg of rifampin per ml (data not shown). Thus, the difference in steady-state amounts of the *pdxH-tyrS* and P_{tyrS} transcripts did not appear to be caused by different transcript stabilities.

The 294-nt band is indicative of a transcription start at position 1048 in Fig. 3. Inspection of the DNA sequence in this region shows that P_{tyrS} is a nonconventional promoter, because it largely lacks −35 and −10 σ-70 consensus regions. Yet P_{tyrS} is about four times stronger than P_{pdxH}, which has relatively good consensus matches (Fig. 3). On the basis of rRNA promoters, it seemed that the unusual relative strength of P_{tyrS} might be accounted for by two upstream features. First, P_{tyrS} is preceded by A-T-rich tracks highly reminiscent of upstream activating sequences of rRNA promoters (Fig. 3) (39). The periodic repetition of A and T residues may indicate that P_{tyrS} is naturally bent DNA (21, 31, 39). Second, two putative Fis protein-binding sites are located directly upstream from P_{tyrS} (Fig. 3) (59). However, P_{tyrS} chromosomal expression was unaffected by a *fis*::*kan* mutation during growth in LBC medium at 37°C (Fig. 6, lane 3).

Requirement for PLP/PMP biosynthesis early in cell division. Growth characteristics of *pdxH*::Mud*I*-8 mutants during mild PL limitation implied that PLP is required for a step early in cell division. *pdxH*::Mud*I*-8 mutants show an absolute requirement for PL that cannot be satisfied by PN (Fig. 1). Although LBC rich medium seems to contain excess PN, we found that it was partially limiting for PL. Colonies of *pdxH*::Mud*I*-8 mutants grew noticeably more slowly on LBC plates at 37°C than their *pdxH*$^+$ parent (Table 2). *pdxH*::Mud*I*-8 mutants grown overnight in LBC medium at 30°C assumed extremely unusual shapes (Fig. 7B). The cells were greatly elongated and contained nucleoids that apparently could not segregate (compare panels A and B, Fig. 7). Several observations support the idea that the elongated cell phenotype was directly due to a limitation of PLP or PMP. Addition of PL, but not D-alanine (2, 19), to LBC medium or the presence of the pTX281 *pdxH*$^+$ minimal clone (Fig. 2) eliminated the defective cell morphology (data not shown). Moreover, the elongated cell phenotype was not caused by the presence of the Mud*I*-8 element, because analogous *pdxA*::Mud*I*-8 mutants did not show defective shape or

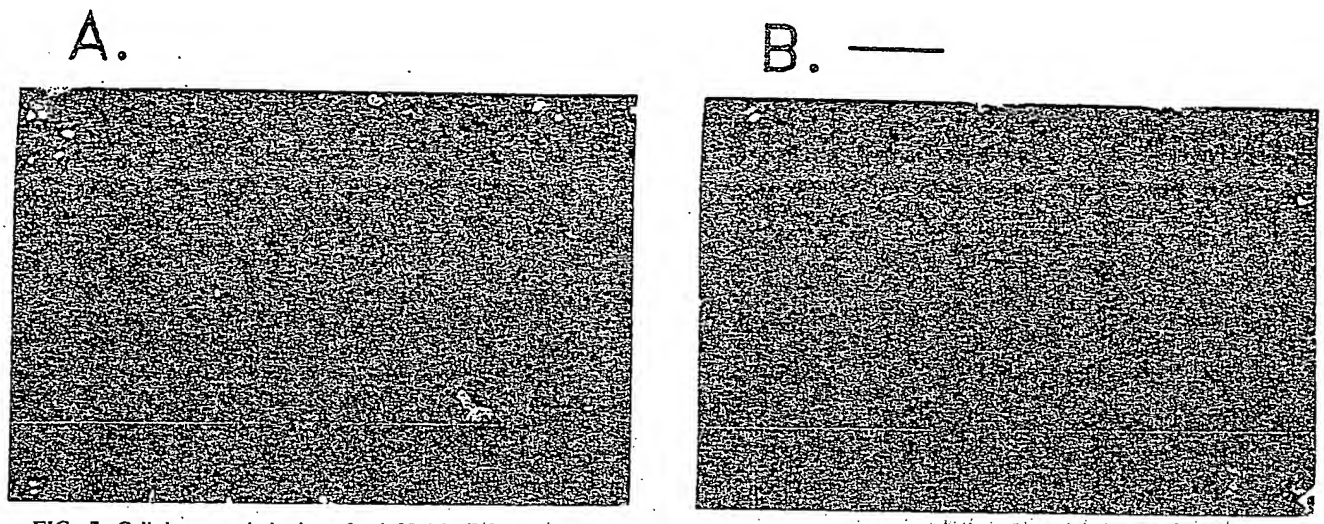

FIG. 7. Cellular morphologies of *pdxH*::Mu*d*I-8 mutant NU1707 in LBC-PL (A) or LBC (B) medium. Cells obtained from overnight cultures grown with shaking at 30°C were washed with 0.84% NaCl, stained with DAPI, and photographed under combined fluorescent and phase-contrast optics as described in Materials and Methods. Similar results were obtained for *pdxH*::Mu*d*I-8 mutant NU1708 (data not shown). Bar, 10 μm. When the *pdxH*$^+$ parent strain or *pdxH*::Mu*d*I-8 mutant NU1707 transformed with *pdxH*$^+$ plasmid pNU216, pNU217, or pTX281 was grown in LBC or LBC-PL medium, all cells resembled those in panel A (i.e., no elongated cells with partially segregated nucleoids were observed; data not shown).

nucleoid segregation (data not shown). The importance of PLP and PMP biosynthesis to cell division is considered further in the Discussion.

Requirement for *pdxH* function but existence of a second pathway for PNP oxidation. The well-characterized *pdxH*::Mu*d*I-8 insertion mutants described above allowed us to examine whether *E. coli* contains one or two forms of PdxH oxidase. In eukaryotes, PNP oxidase seems to show an absolute requirement for molecular oxygen as an electron acceptor (29, 40). Therefore, we wondered whether facultative anaerobes, such as *E. coli*, contain two forms of PNP oxidase or a single PNP oxidase with the ability to use electron acceptors other than oxygen. To test the former hypothesis, we determined whether *pdxH*::Mu*d*I-8 mutants could grow anaerobically in the absence of added PL. The results show that *pdxH*::Mu*d*I-8 mutants require PL under all growth conditions (Table 2).

The structural data presented above show that *pdxH*::Mu*d*I-8 insertions are at most only moderately polar on downstream gene expression (about 20%) because of P_{tyrS} (Fig. 6). In addition, transcription downstream of *tyrS* probably occurs from the opposite DNA strand from *pdxH* and *tyrS*, which means that *tyrS* is the last gene in what appears to be a two-gene complex operon (Fig. 2 and see above). Thus, it seemed extremely unlikely that *pdxH*::Mu*d*I-8 insertions were exerting a polar effect on a downstream, anaerobic *pdxH* gene. To test this notion further, we transformed the *pdxH*$^+$ parent NU816 and *pdxH*::Mu*d*I-8 mutants NU1707 and NU1708 with the three *pdxH*$^+$ plasmids depicted in Fig. 2. Surprisingly, pNU217 and minimal *pdxH*$^+$ clone pTX281 inhibited and pNU216 prevented anaerobic growth of both the parent and *pdxH* mutants in Casamino Acid-supplemented MMG lacking antibiotics (Table 2). When larger colonies did appear, the bacteria had lost the *pdxH*$^+$ plasmids. By contrast, on LBC rich medium, the plasmids did not adversely affect growth. Control experiments indicated that the pBR325 vector did not adversely affect anaerobic growth of the NU816 parent strain (data not shown). Thus, *pdxH*$^+$ itself and other genes nearby cannot be tolerated on multicopy plasmids in bacteria growing anaerobically on enriched minimal-glucose medium.

Last, we tested whether suppressors could be isolated in *pdxH*::Mu*d*I-8 mutants that allow aerobic or anaerobic growth on minimal media lacking PL. Unexpectedly, stable, spontaneous suppressors could be isolated both in the presence and absence of oxygen. *pdxH* suppressors isolated under aerobic conditions allowed anaerobic growth without PL and vice versa (data not shown). Preliminary cotransduction mapping revealed at least two classes of suppressors, linked or unlinked to the *pdxH* region, which were isolated most readily under anaerobic or aerobic conditions, respectively (data not shown). Implications to PLP biosynthesis of suppressors that replace *pdxH* oxidase function are considered in the Discussion.

***pdxH*::Mu*d*I-8 mutants excrete significant amounts of L-Glu and a compound that triggers L-valine inhibition of *E. coli* K-12 strains.** Mutations in *pdxH* lead to accumulation of precursors in the PLP biosynthetic pathway, such as PNP and PMP (Fig. 1). We observed that *pdxH*::Mu*d*I-8 liquid cultures grew about a third as fast as the *pdxH*$^+$ parent strain in MMG-PL at 30°C (data not shown). When *pdxH*::Mu*d*I-8 mutants were streaked side by side with their *E. coli* K-12 parent strain on MMG-PL plates, a striking inhibition of the parent strain was obvious (data not shown). These results strongly hinted that *pdxH*::Mu*d*I-8 mutants were excreting a growth inhibitor into the culture medium.

To investigate this phenomenon further, cell-free filtrates were made from cultures of *pdxH*::Mu*d*I-8 mutants (Table 3). Ten microliters of filtrate from overnight cultures was sufficient to cause a 1- to 2-cm-diameter inhibition zone for K-12 strain NU816. Because inhibition was observed only on MMG agar but not on LBC rich agar, it seemed that the inhibitor might be acting on some biosynthetic process. Moreover, production of inhibitor was due solely to the *pdxH* mutations, since no inhibition was observed for

TABLE 3. Growth inhibition by medium filtrates of *pdxH*::Mud*I*-8 mutants

Filtrate source[a]	Diam of inhibition zone (cm) of[b]:					
	E. coli K-12		*E. coli* B		Filtrate-resistant K-12 mutant	
	−Ile	+Ile	−Ile	+Ile	−Ile	+Ile
pdxH$^+$ parent (NU816)	0	NT	0	NT	NT	NT
pdxH::Mud*I*-8 mutants						
NU1707	1.4	0	0	0	0	0
NU1708	2.2	0	0	0	0	0
pdxA::Mud*I*-8 (NU1709)	0	NT	NT	NT	NT	NT
pdxH::Mud*I*-8 mutants with recombinant *pdxH*$^+$ plasmids	0	NT	NT	NT	NT	NT
Chemicals (mg/ml)						
L-Val						
0.3	1.8	0	0	0	0	0
0.03	1.1	0	0	0	0	0
0.003	0	0	0	0	0	0
L-Glu (3)	0	NT	NT	NT	NT	NT
L-Val + L-Glu						
0.03 + 3	1.1	NT	NT	NT	NT	NT
0.003 + 3	0	NT	NT	NT	NT	NT
α-KIV						
0.3	2.1	0	NT	NT	NT	NT
0.03	1.2	0	NT	NT	NT	NT

[a] Cultures used to prepare filtrates were grown in MMG-PL at 30°C for 3 days (*pdxH*::Mud*I*-8 mutants) or 1 to 2 days (other strains). Ampicillin (12.5 μg/ml) was added to all cultures except NU816. Cells were then removed by low-speed centrifugation followed by filtration through 0.2-μm-pore-size filters.

[b] Cultures of the three strains to be tested were grown in MMG overnight at 37°C. The overnight culture (0.1 ml) was mixed with 0.8% MMG soft agar and poured onto 1.5% MMG bottom agar. Both top and bottom agars contained 0.3 mM L-Ile, where indicated. Inhibition caused by cell filtrates and various chemicals was tested by adding 10 μl of filtrates or chemical solutions at the concentrations listed to sterile filter paper discs placed on plate surfaces immediately after the agar hardened. Plates were inverted and incubated at 37°C for 1 day before inhibition zones were measured. NT, not tested.

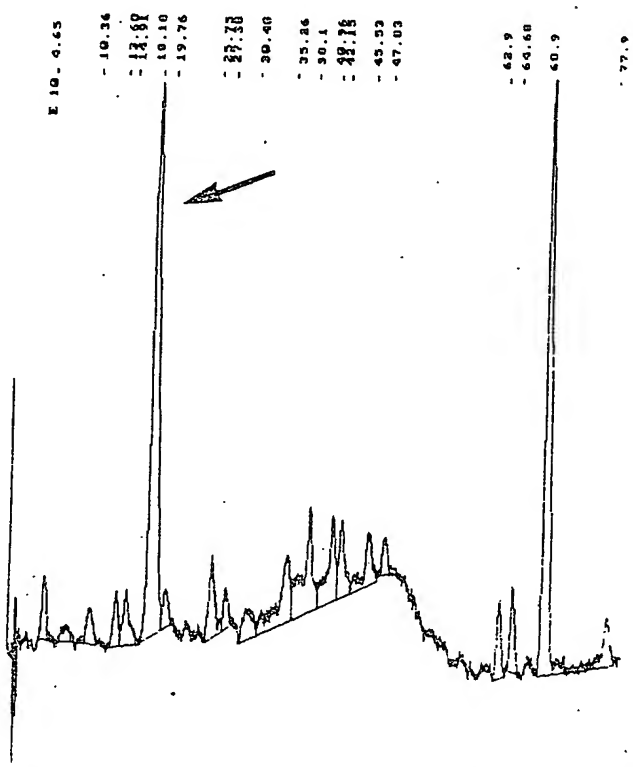

FIG. 8. HPLC analysis of amino acids contained in cell filtrates of a *pdxH*::Mud*I*-8 mutant (NU1708) grown in MMG-PL at 37°C with shaking. Cell filtrates were prepared as described in Table 2, footnote *a*. The sterile conditioned medium was further filtered through a Centricon 3 filter (Amicon Corp., Beverly, Mass.) to remove molecules with molecular masses greater than 3,500 Da. This extra filtration did not appear to diminish the filtrate's ability to inhibit *E. coli* K-12 (data not shown). The final filtrate was mixed with low concentrations of amino acid standards to help identify peaks and subjected to HPLC ion-exchange chromatography as described in Materials and Methods. The large peak at 18.18 min (arrow) represents L-Glu. The other large peak at 68.9 min is ammonium ion. The L-Val standard is at 35.26 min. Only the two large peaks were observed on chromatograms of conditioned medium lacking the amino acid standards (data not shown). Additional details and controls are described in the text.

pdxA::Mud*I*-8 or *pdxH*::Mud*I*-8 (*pdxH*$^+$ plasmid) strains (Table 3).

L-Valine is a well-known metabolic inhibitor of *E. coli* K-12 growth that acts by feedback inhibiting isozymes I and III of acetohydroxy acid synthase (57). The following properties of the culture filtrates strongly suggested that the excreted inhibitor was L-Val or a compound related to L-Val (Table 3): (i) L-Ile reversed the inhibitory effect, (ii) *E. coli* K-12, but not *E. coli* B, cells were inhibited, and (iii) 2-aminopurine mutagenized *E. coli* K-12 mutants selected for resistance to the *pdxH* mutant filtrates were also resistant to L-Val inhibition.

We tested whether *pdxH* mutants were excreting L-Val by performing amino acid analyses on filtrates (Fig. 8). The MMG-PL culture filtrate of *pdxH* mutant NU1707 or NU1708 was mixed with a low concentration of amino acid standards to pinpoint relative peak positions. The resulting chromatograms showed two major peaks corresponding to ammonium ion and L-glutamate (arrow, Fig. 8) but no peak of L-Val (Fig. 8). When amino acid standards were omitted, only the ammonium and L-glutamate peaks were seen (data not shown). Inhibition zone tests with pure L-Val suggested that if L-Val were present, it would have a minimal concentration of approximately 0.03 mg/ml (Table 3). This concentration was well within the range of detection of the amino acid analyses (data not shown).

Excretion of L-Glu by *pdxH*::Mud*I*-8 mutants was totally unanticipated (Fig. 8). L-Glu was not detected in filtrates of the *pdxH*$^+$ parent (NU816) or *pdxH*::Mud*I*-8 mutants containing a *pdxH*$^+$ recombinant plasmid (NU2352 and NU2353) (data not shown). The presence of L-Glu in culture filtrates was confirmed further with a bioassay employing the enzyme glutamate dehydrogenase, which specifically uses L-Glu as its substrate (6). Our results showed that NU1708 (*pdxH*), but not NU816 (*pdxH*$^+$), filtrates indeed contained a substrate of glutamate dehydrogenase (data not shown). Based on the amino acid analyses, the concentration of L-Glu in NU1708 filtrates was about 1 nmol/μl (≈0.15 mg/ml). The effects of pure L-Glu on the growth of *E. coli* K-12 strains were also tested. No inhibition zone was seen even with L-Glu concentrations as high as 3 mg/ml. In addition, L-Glu did not enhance the inhibitory effect of L-Val (Table 3). On the basis of these results, L-Glu was not the inhibitor of *E. coli* K-12 growth excreted by *pdxH* mutants.

Since L-Val was not excreted and L-Glu did not act as an inhibitor, it seemed likely that a precursor of L-Val lacking a free amino group might be the inhibitor released by *pdxH* mutants. Such a precursor could then be taken up by *E. coli* K-12 strains and converted directly into L-Val, thereby eliciting inhibition. To account for the simultaneous excretion of L-Glu and this precursor, we hypothesized that PNP/PMP accumulation in *pdxH* mutants (Fig. 1) inhibits the activity of transaminases, which use L-Glu as a common substrate. In the L-Val biosynthetic pathway, blockage of the transaminase reaction would lead to accumulation and possibly excretion of the keto acid α-ketoisovalerate (α-KIV). Consistent with this hypothesis, we found that α-KIV inhibited the growth of *E. coli* K-12 cells in a manner similar to L-Val (Table 3).

DISCUSSION

PNP oxidase, which catalyzes the last step in PLP biosynthesis in all organisms (Fig. 1), has been extensively characterized biochemically in animal tissues (10, 11, 29, 36). In this paper, we report a molecular genetic analysis of *pdxH*, which encodes PNP oxidase in *E. coli* K-12. These studies revealed significant new information about the function, genetic organization, and physiological role of *E. coli* PdxH oxidase.

We found several similarities between *E. coli* and eukaryotic PNP oxidases. The predicted monomer molecular mass of the *E. coli* polypeptide was 25,545 Da (Fig. 3), which is similar to that of the eukaryotic enzyme. Likewise, the predicted amino acid composition of *E. coli* PdxH oxidase (Fig. 3) was similar to that of eukaryotic enzymes, which were determined biochemically (36). The *E. coli* PdxH polypeptide is predicted to be basic (pI≈9.6) and to contain a relatively high number of polar amino acids compared to aromatic and sulfur-containing residues. *E. coli* PNP oxidase probably binds FMN, as indicated by its full-length homology with the FMN-binding FprA protein of *M. xanthus* (Fig. 4) (20). It is well established that eukaryotic PNP oxidases use FMN as a cofactor (11). Furthermore, the high degree (>40% identity) and nearly full-length homology between PdxH and FprA is striking (Fig. 4) and strongly implies that FprA is PNP oxidase of *M. xanthus*.

One fundamental difference between the *E. coli* and eukaryotic oxidases may concern function during anaerobic growth. Eukaryotic PdxH oxidases are thought to utilize molecular oxygen as their sole electron acceptor (29, 40). Our genetic analyses show that PdxH oxidase is required in wild-type *E. coli* K-12 for both aerobic and anaerobic growth (Table 2). Consistent with this interpretation, crude extracts from the NU1708 *pdxH*::Mu*dI*-8 insertion mutant totally lack the PNP oxidase activity, which is easily detectable from its *pdxH*$^+$ parent (66). However, the existence of suppressors of *pdxH* function in *pdxH* insertion mutants (see Results) suggests a more complicated situation. One possibility is that there is a single form of PdxH oxidase in wild-type *E. coli*, which uses oxygen aerobically and another electron acceptor anaerobically. In this case, *pdxH* suppressors arise by mutational change in specificity of a pathway that does not normally participate in PNP oxidation. Alternatively, a cryptic pathway for PNP oxidation might be activated. A second possibility is that PdxH protein is the aerobic oxidase that is nevertheless required for activation of a second, anaerobic form of the enzyme. According to this model, *pdxH* suppressors arise because of constitutive expression of the second form of oxidase. Enzymological characterization of *E. coli* PdxH and molecular genetic analysis of *pdxH* suppressors are in progress to test these models.

Genetic, structural, and in vivo transcript analyses revealed that *pdxH* forms a complex operon with downstream *tyrS* (Fig. 2, 3, 5, and 6). In LBC medium at 37°C with aeration, approximately 20 or 80% of steady-state *tyrS* transcripts seemed to originate from the *pdxH* (P_{pdxH}) or *tyrS* (P_{tyrS}) promoters, respectively (Fig. 2, 3, 5, and 6). No transcription was detected in either direction in the 280-bp region immediately upstream from the start of *pdxH* transcription, although this region contained an open reading frame (ORF1, Fig. 2 and 3). Gene fusions immediately downstream from *tyrS* indicated that this region is transcribed in the opposite direction to *tyrS* (Fig. 2). Thus, *pdxH* and *tyrS* form a two-gene complex operon that contains a relatively strong internal promoter (P_{tyrS}). This conclusion means that all known genes involved in PN (vitamin B_6) or PLP biosynthesis are members of a complex, multifunctional operon (2, 17, 33, 34, 44, 54). Besides *tyrS*, other aminoacyl-tRNA synthetase genes have also been found in complex operons (27, 28, 35). One model to explain this arrangement is that complex operons may allow coordinated or differential expression of key metabolic functions depending on the physiological state of the cell. In this regard, it is interesting that *pdxA*, *pdxB*, and now *pdxH* are in complex operons with genes that encode proteins important for translation, and *pdxJ* is in a complex operon with a recently discovered essential gene of unknown function (33, 54).

The regulation of *tyrS* has not been extensively studied in *E. coli*. On the basis of precedents from other aminoacyl-tRNA synthetase genes, *tyrS* may be regulated positively by growth rate and perhaps by tyrosine limitation (38). *Bacillus subtilis tyrS* is induced by tyrosine starvation possibly through a mechanism involving antitermination (61). The results presented here suggest that *E. coli tyrS* is transcribed mainly from a relatively powerful, nonconventional internal promoter that shares features with rRNA promoters (39) (Fig. 3). Although P_{tyrS} lacks strong −35 and −10 consensus sequences, it is preceded by A-T-rich DNA that likely is naturally bent (21, 31, 39) and contains two potential Fis protein-binding sites (59). However, in vivo transcription from P_{tyrS} was unaffected by a *fis*::*kan* mutation (Fig. 6), which is a property shown by several other promoters that bind Fis in vitro (65). P_{pdxH} accounts for *pdxH* and about 20% of *tyrS* transcription (Fig. 5 and 6) and appears to be a conventional σ-70 promoter. PDX boxes, found near the starts of *pdxA*, *pdxB*, and *pdxJ* (33, 44, 49), and other putative regulatory motifs were not discernable around P_{pdxH} or within *pdxH*. Ongoing experiments should determine whether relative steady-state amounts or rates of transcription from P_{pdxH} and P_{tyrS} change under different growth conditions.

pdxH::Mu*dI*-8 insertion mutants showed several unusual phenotypic properties that seemed to be due directly to PLP coenzyme level rather than partial polarity on *tyrS* expression. When *pdxH* mutants ran out of PL in LBC rich medium, they showed a pronounced division defect characterized by elongated large cells with unsegregated nucleoids (Fig. 7). This appearance contrasts with the spherical cell and swelling and bleb phenotypes caused by severe PLP limitation that presumably reflects blockage of peptidoglycan biosynthesis (2, 19). The cell division defect reported here was not lessened by D-alanine addition and may not reflect a block in murein biosynthesis (2, 19). The unsegregated nucleoids in mildly PLP-limited *pdxH* mutants suggest

that some early step in cell division requires PLP (12, 16). This conclusion implies that *E. coli* needs to carefully regulate PLP level throughout the cell cycle. Consistent with this interpretation, *pdxA* and *pdxB*, which are required for PN and PLP biosynthesis (2, 44), are positively regulated by growth rate at the level of transcription initiation (43). In this regard, it is interesting that *fprA*, which we show probably encodes PNP oxidase (Fig. 4), has been reported to be developmentally regulated in *M. xanthus* (20). If this interpretation is correct, PLP coenzyme level may be modulated as a function of developmental stage in *M. xanthus*.

Excretion of appreciable amounts of L-glutamate and a precursor of L-valine by *pdxH* mutants in media containing PL (Fig. 8; Table 3) underscores the importance to cells of maintaining appropriate pool levels of PLP precursors. *pdxH* mutants most likely accumulate PNP and PMP, which are substrates of PNP oxidase (Fig. 1). PNP and PMP are known to be potent inhibitors of PLP-dependent enzymes, including transaminases (52), and transaminases utilize L-Glu as a common substrate (5). We speculate that PNP and PMP accumulation by *pdxH* mutants inhibits transaminases and leads to the accumulation and excretion of transaminase substrates, including L-Glu and α-keto acids, such as the immediate precursor of L-Val, α-KIV. This hypothesis has two implications. First, under some circumstances, cellular PNP or PMP concentrations control the activity of certain enzymes and thereby regulate the flow of intermediates in certain metabolic pathways. Second, excretion of L-Glu implies an unanticipated breakdown in feedback regulation of L-Glu biosynthesis (42). In this case, the PNP level may affect metabolic flow by altering the efficiency of feedback control. Whether PNP and PLP levels are modulated in *pdxH*$^+$ bacteria under different growth conditions awaits testing.

ACKNOWLEDGMENTS

We thank the colleagues listed in Table 1 for bacterial strains and plasmid clones. Tsz-Kwong Man provided valuable assistance in the analysis of *pdxH* suppressors. We also thank D. M. Connolly, W. B. Dempsey, H.-C. E. Leung, A. J. Pease, B. B. Roa, H.-C. T. Tsui, and G. Zhao for discussions and comments.

This work was supported by Public Health Service grant GM37561 from the National Institute of General Medical Sciences.

REFERENCES

1. **Arps, P. J., and M. E. Winkler.** 1987. Structural analysis of the *Escherichia coli* K-12 *hisT* operon by using a kanamycin resistance cassette. J. Bacteriol. 169:1061–1070.
2. **Arps, P. J., and M. E. Winkler.** 1987. An unusual genetic link between vitamin B_6 biosynthesis and tRNA pseudouridine modification in *Escherichia coli* K-12. J. Bacteriol. 169:1071–1079.
3. **Ausubel, F. M., R. Brent, R. E. Kingston, D. D. Moore, J. G. Seidman, J. A. Smith, and K. Struhl.** 1989. Current protocols in molecular biology. Wiley Interscience, New York.
4. **Barker, D. G., C. J. Bruton, and G. Winter.** 1982. The tyrosyl-tRNA synthetase from *Escherichia coli*. Complete nucleotide sequence of the structural gene. FEBS Lett. 150:419–423.
5. **Bender, D. A.** 1985. Amino acid metabolism. John Wiley & Sons, Inc., New York.
6. **Bernt, E., and H.-U. Bergmeyer.** 1965. L-Glutamate: determination with glutamic dehydrogenase, p. 384–388. *In* H.-U. Bergmeyer (ed.), Methods of enzymatic analysis. Academic Press, Inc., New York.
7. **Birktoft, J. J., and L. J. Banaszak.** 1984. Structure-function relationships among nicotinamide-adenine dinucleotide oxidoreductases. Peptide Protein Rev. 4:1–46.
8. **Bolivar, F.** 1978. Construction and characterization of new cloning vehicles. III. Derivatives of plasmid pBR322 carrying unique *Eco*RI generated recombinant molecules. Gene 2:95–113.
9. **Castilho, B. A., P. Olfson, and M. J. Casadaban.** 1984. Plasmid insertion mutagenesis and *lac* gene fusion with mini-Mu bacteriophage transposons. J. Bacteriol. 158:488–495.
10. **Choi, S.-Y., J. E. Churchich, E. Zaiden, and F. Kwok.** 1987. Brain pyridoxine-5-phosphate oxidase: modulation of its catalytic activity by reaction with pyridoxal 5-phosphate and analogs. J. Biol. Chem. 262:12013–12017.
11. **Churchich, J. E.** 1984. Brain pyridoxine-5-phosphate oxidase. A dimeric enzyme containing one FMN site. Eur. J. Biochem. 138:327–332.
12. **Cooper, S.** 1991. Bacterial growth and division: biochemistry and regulation of prokaryotic and eukaryotic division cycles. Academic Press, Inc., New York.
13. **Davis, R. W., D. Botstein, and J. R. Roth.** 1980. Advanced bacterial genetics. Cold Spring Harbor Laboratory, Cold Spring Harbor, N.Y.
14. **Dempsey, W. B.** 1966. Synthesis of pyridoxine by a pyridoxal auxotroph of *Escherichia coli*. J. Bacteriol. 92:333–337.
15. **Dempsey, W. B.** 1987. Synthesis of pyridoxal phosphate, p. 539–543. *In* F. C. Neidhardt, J. L. Ingraham, K. B. Low, B. Magasanik, M. Schaechter, and H. E. Umbarger (ed.), *Escherichia coli* and *Salmonella typhimurium*: cellular and molecular biology. American Society for Microbiology, Washington, D.C.
16. **Donachie, W. D., K. J. Begg, and N. F. Sullivan.** 1984. Morphogenes of *Escherichia coli*, p. 27–62. *In* R. Losick and L. Shapiro (ed.), Microbial development. Cold Spring Harbor Laboratory, Cold Spring Harbor, N.Y.
17. **Duncan, K., and J. R. Coggins.** 1986. The *serC-aroA* operon of *Escherichia coli*: a mixed function operon encoding enzymes from two different amino acid biosynthetic pathways. Biochem. J. 234:49–57.
18. **Erickson, J. W., V. Vaughn, W. A. Walter, F. C. Neidhardt, and C. A. Gross.** 1987. Regulation of the promoters and transcripts of *rpoH*, the *Escherichia coli* heat shock regulatory gene. Genes Dev. 1:419–432.
19. **Grogan, D. W.** 1988. Temperature-sensitive murein synthesis in an *Escherichia coli pdx* mutant and the role of alanine racemase. Arch. Microbiol. 150:363–367.
20. **Hagen, T. J., and L. J. Shimkets.** 1990. Nucleotide sequence and transcriptional products of the *csg* locus of *Myxococcus xanthus*. J. Bacteriol. 172:15–23.
21. **Hagerman, P. J.** 1986. Sequence-directed curvature of DNA. Nature (London) 321:449–450.
22. **Hedrick, J. L., and E. H. Fischer.** 1965. On the role of pyridoxal 5′-phosphate in phosphorylase. I. Absence of classical vitamin B_6-dependent enzymatic activities in muscle glycogen phosphorylase. Biochemistry 4:1337–1342.
23. **Hill, R. E., B. G. Sayer, and I. D. Spenser.** 1989. Biosynthesis of vitamin B_6: incorporation of D-1-deoxyxylulose. J. Am. Chem. Soc. 111:1916–1917.
24. **Hiraga, S., H. Niki, T. Ogura, C. Ichinose, H. Mori, B. Ezaki, and A. Jaffe.** 1989. Chromosome partitioning in *Escherichia coli*: novel mutants producing anucleate cells. J. Bacteriol. 171:1496–1505.
25. **Hockney, R. C., and T. Scott.** 1979. The isolation and characterization of three types of vitamin B6 auxotrophs of *Escherichia coli* K12. J. Gen. Microbiol. 110:275–283.
26. **Hughes, K. T., and J. R. Roth.** 1989. Conditionally transposition-defective derivative of Mu *d*1(Amp Lac). J. Bacteriol. 159:130–137.
27. **Kamio, Y., C.-K. Lin, M. Regue, and H. C. Wu.** 1985. Characterization of the *ileS-lsp* operon in *Escherichia coli*: identification of an open reading frame upstream of the *ileS* gene and potential promoter(s) for the *ileS-lsp* operon. J. Biol. Chem. 260:5616–5620.
28. **Kawakami, K., Y. H. Jonsson, G. R. Bjork, H. Ikeda, and Y. Nakamura.** 1988. Chromosomal location and structure of the operon encoding peptide-chain-release factor 2 of *Escherichia coli*. Proc. Natl. Acad. Sci. USA 85:5620–5624.
29. **Kazarinoff, M. N., and D. B. McCormick.** 1975. Rabbit liver pyridoxamine (pyridoxine) 5′-phosphate oxidase. Purification and properties. J. Biol. Chem. 250:3436–3442.

30. **Kim, Y. T., and J. E. Churchich.** 1989. Activation of a flavoprotein by proteolysis. J. Biol. Chem. **264**:15751–15753.
31. **Koo, H.-S., H.-M. Wu, and D. M. Crothers.** 1986. DNA bending at adenine-thymine tract. Nature (London) **320**:501–506.
32. **Kwok, F., and J. E. Churchich.** 1980. Interaction between pyridoxal kinase and pyridoxine-5-P oxidase, two enzymes involved in the metabolism of vitamin B_6. J. Biol. Chem. **255**:882–887.
33. **Lam, H.-M., E. Tancula, W. B. Dempsey, and M. E. Winkler.** 1992. Suppression of insertions in the complex *pdxJ* operon of *Escherichia coli* K-12 by *lon* and other mutations. J. Bacteriol. **174**:1554–1567.
34. **Lam, H.-M., and M. E. Winkler.** 1990. Metabolic relationships between pyridoxine (vitamin B_6) and serine biosynthesis in *Escherichia coli* K-12. J. Bacteriol. **172**:6518–6528.
35. **Mayaux, J.-F., G. Fayat, M. Fromant, M. Springer, M. Grunberg-Manago, and S. Blanquet.** 1983. Structural and transcriptional evidence for related *thrS* and *infC* expression. Proc. Natl. Acad. Sci. USA **80**:6152–6156.
36. **McCormick, D. B., and A. H. Merrill.** 1980. Pyridoxamine (pyridoxine) 5′-phosphate oxidase, p. 1–26. *In* G. P. Tryfiates (ed.), Vitamin B6 metabolism and role in growth. Food Nutrition Press, Westport, Conn.
37. **Miller, J. H.** 1972. Experiments in molecular genetics. Cold Spring Harbor Laboratory, Cold Spring Harbor, N.Y.
38. **Neidhardt, F. C., J. Parker, and W. G. McKeever.** 1975. Function and regulation of aminoacyl-tRNA synthetases in prokaryotic and eukaryotic cells. Annu. Rev. Microbiol. **29**: 215–250.
39. **Plaskon, R. R., and R. M. Wartell.** 1987. Sequence distributions associated with DNA curvature are found upstream of strong *E. coli* promoters. Nucleic Acids Res. **15**:785–796.
40. **Pogell, B. M.** 1958. Enzymatic oxidation of pyridoxamine phosphate to pyridoxal phosphate in rabbit liver. J. Biol. Chem. **232**:761–776.
41. **Porter, T. D., and C. B. Kasper.** 1986. NADPH-cytochrome P-450 oxidoreductase: flavin mononucleotide and flavin adenine dinucleotide domains evolved from different flavoproteins. Biochemistry **25**:1682–1687.
42. **Reitzer, L. J., and B. Magasanik.** 1987. Ammonia assimilation and the biosynthesis of glutamine, glutamate, aspartate, asparagine, L-alanine, and D-alanine, p. 302–320. *In* F. C. Neidhardt, J. L. Ingraham, K. B. Low, B. Magasanik, M. Schaechter, and H. E. Umbarger (ed.), *Escherichia coli* and *Salmonella typhimurium*: cellular and molecular biology. American Society for Microbiology, Washington, D.C.
43. **Roa, B. B., K. Betchel, and M. E. Winkler.** 1992. Unpublished observation.
44. **Roa, B. B., D. M. Connolly, and M. E. Winkler.** 1989. Overlap between *pdxA* and *ksgA* in the complex *pdxA-ksgA-apaG-apaH* operon of *Escherichia coli* K-12. J. Bacteriol. **171**:4767–4777.
45. **Rudd, K. E.** Alignment of *E. coli* DNA sequences to a revised, integrated genomic restriction map. *In* J. Miller (ed.), A short course in bacterial genetics: a laboratory manual and handbook of *Escherichia coli* and related bacteria, in press. Cold Spring Harbor Laboratory Press, Cold Spring Harbor, N.Y.
46. **Sambrook, J., E. F. Fritsch, and T. Maniatis.** 1989. Molecular cloning: a laboratory manual, 2nd ed. Cold Spring Harbor Laboratory, Cold Spring Harbor, N.Y.
47. **Sanger, F., S. Nicklen, and A. R. Coulson.** 1977. DNA sequencing with chain-terminating inhibitors. Proc. Natl. Acad. Sci. USA **74**:5463–5467.
48. **Schlesinger, S., and E. W. Nester.** 1969. Mutants of *Escherichia coli* with an altered tyrosyl-transfer ribonucleic acid synthetase. J. Bacteriol. **100**:167–175.
49. **Schoenlein, P. V., B. B. Roa, and M. E. Winkler.** 1989. Divergent transcription of *pdxB* and homology between the *pdxB* and *serA* gene products in *Escherichia coli* K-12. J. Bacteriol. **171**:6084–6092.
50. **Shimkets, L. J.** 1990. The *Myxococcus xanthus* FprA protein causes increased flavin biosynthesis in *Escherichia coli*. J. Bacteriol. **172**:24–30.
51. **Snell, E. E.** 1955. Chemical structure in relation to biological activities of vitamin B_6. Vitam. Horm. **16**:77–113.
52. **Spencer, M. E., and J. R. Guest.** 1974. Proteins of the inner membrane of *Escherichia coli*: changes in composition associated with anaerobic growth and fumerate reductase amber mutations. J. Bacteriol. **117**:954–959.
53. **Stockman, B. J., A. M. Krezel, and J. L. Markley.** 1990. Hydrogen-1, carbon-13, and nitrogen-15 NMR spectroscopy of *Anabaena* 7120 flavodoxin: assignment of beta-sheet and flavin binding site resonances and analysis of protein-flavin interactions. Biochemistry **29**:9600–9609.
54. **Takiff, H. E., T. Baker, T. Copeland, S.-M. Chen, and D. L. Court.** 1992. Locating essential *Escherichia coli* genes by using mini-Tn*10* transposons: the *pdxJ* operon. J. Bacteriol. **174**:1544–1553.
55. **Tryfiates, G. P.** 1986. Pyridoxal phosphate and metabolism, p. 421–448. *In* D. Dolphin, R. Poulson, and O. Avramovic (ed.), Vitamin B_6 pyridoxal phosphate, part B. Wiley Interscience, New York.
56. **Turner, J. M., and F. C. Happold.** 1961. Pyridoxamine phosphate-oxidase and pyridoxal phosphate-phosphatase activities in *Escherichia coli*. Biochem. J. **78**:364–372.
57. **Umbarger, H. E.** 1987. Biosynthesis of the branched-chain amino acids, p. 352–367. *In* F. C. Neidhardt, J. L. Ingraham, K. B. Low, B. Magasanik, M. Schaechter, and H. E. Umbarger (ed.), *Escherichia coli* and *Salmonella typhimurium*: cellular and molecular biology. American Society for Microbiology, Washington, D.C.
58. **Uyeda, K.** 1969. Reaction of phosphofructokinase with maleic anhydride, succinic anhydride, and pyridoxal 5′-phosphate. Biochemistry **8**:2366–2373.
59. **Verbeek, H., L. Nilsson, G. Baliko, and L. Bosch.** 1990. Potential binding sites of the trans-activator FIS are present upstream of all rRNA operons and of many but not all tRNA operons. Biochim. Biophys. Acta **1050**:302–306.
60. **Wada, H., and E. E. Snell.** 1961. The enzymatic oxidation of pyridoxine and pyridoxamine phosphates. J. Biol. Chem. **236**: 2089–2095.
61. **Waye, M. M. Y., and G. Winter.** 1986. A transcription terminator in the 5′ non-coding region of the tyrosyl tRNA synthetase gene from *Bacillus stearothermophilus*. Eur. J. Biochem. **158**: 505–510.
62. **White, R. S., and W. B. Dempsey.** 1970. Purification and properties of vitamin B_6 kinase from *Escherichia coli* B. Biochemistry **9**:4057–4064.
63. **Winans, S. C., S. J. Elledge, J. H. Krueger, and G. C. Walker.** 1985. Site-directed insertion and deletion mutagenesis with cloned fragments in *Escherichia coli*. J. Bacteriol. **161**:1219–1221.
64. **Yasunobu, K. T., and M. Tanaka.** 1980. The isolation and primary structures of various types of ferredoxin. Methods Enzymol. **69**:228–238.
65. **Zacharias, M., H. U. Goringer, and R. Wagner.** 1992. Analysis of the Fis-dependent and Fis-independent transcription activation mechanisms of the *Escherichia coli* ribosomal RNA P1 promoter. Biochemistry **31**:2621–2628.
66. **Zhao, G., and M. E. Winkler.** 1992. Unpublished observation.

doi:10.1006/jmbi.2001.5254 available online at http://www.idealibrary.com on IDEAL J. Mol. Biol. (2002) 315, 385–397

JMB

Active Site Structure and Stereospecificity of *Escherichia coli* Pyridoxine-5′-phosphate Oxidase

Martino L. di Salvo[1], Tzu-Ping Ko[2], Faik N. Musayev[3], Samanta Raboni[3] Verne Schirch[3] and Martin K. Safo[3]*

[1]*Dipartimento di Scienze Biochimiche "A. Rossi Fanelli" and Centro di Biologia Molecolare del Consiglio Nazionale delle Ricerche Università La Sapienza, Rome Italy*

[2]*Institute of Biological Chemistry, Academia Sinica Taipei 11529, Taiwan*

[3]*Institute for Structural Biology and Drug Discovery, Virginia Commonwealth University Richmond, VA 23219, USA*

**Corresponding author*

Pyridoxine-5′-phosphate oxidase catalyzes the oxidation of either the C4′ alcohol group or amino group of the two substrates pyridoxine 5′-phosphate and pyridoxamine 5′-phosphate to an aldehyde, forming pyridoxal 5′-phosphate. A hydrogen atom is removed from C4′ during the oxidation and a pair of electrons is transferred to tightly bound FMN. A new crystal form of the enzyme in complex with pyridoxal 5′-phosphate shows that the N-terminal segment of the protein folds over the active site to sequester the ligand from solvent during the catalytic cycle. Using (4′R)-[^{3}H]PMP as substrate, nearly 100% of the radiolabel appears in water after oxidation to pyridoxal 5′-phosphate. Thus, the enzyme is specific for removal of the *pro*R hydrogen atom from the prochiral C4′ carbon atom of pyridoxamine 5′-phosphate. Site mutants were made of all residues at the active site that interact with the oxygen atom or amine group on C4′ of the substrates. Other residues that make interactions with the phosphate moiety of the substrate were mutated. The mutants showed a decrease in affinity, but exhibited considerable catalytic activity, showing that these residues are important for binding, but play a lesser role in catalysis. The exception is Arg197, which is important for both binding and catalysis. The R197 M mutant enzyme catalyzed removal of the *pro*S hydrogen atom from (4′R)-[^{3}H]PMP, showing that the guanidinium side-chain plays an important role in determining stereospecificity. The crystal structure and the stereospecificity studies suggests that the pair of electrons on C4′ of the substrate are transferred to FMN as a hydride ion.

© 2002 Academic Press

Keywords: pyridoxine-5′-phosphate oxidase; pyridoxal 5′-phosphate; pyridoxamine 5′-phosphate; X-ray crystallography; flavin mononucleotide

Introduction

The terminal step in the biosynthesis of pyridoxal 5′-phosphate (PLP) in *Escherichia coli* is the oxidation of pyridoxine 5′-phosphate (PNP) to PLP, which is catalyzed by pyridoxine phosphate oxidase (PNPOx).[1,2] PLP is used to activate a wide variety of apoenzymes involved in amino acid metabolism, as well as enzymes in several other metabolic pathways. In mammalian systems, which do not synthesize PLP, PNPOx is an important step in a PLP salvage pathway. In addition to using PNP as a substrate, the enzymes from both *E. coli* and eukaryotic sources catalyze the oxidation of pyridoxamine 5′-phosphate (PMP) to PLP.[1,3]

PNPOx has been purified from sheep and pig brain, rabbit liver, and *E. coli*.[1,3–7] The most extensive studies have been done with the rabbit liver enzyme.[3,4,8–15] Recently, crystal structures for the *E. coli* enzyme have been published with and without PLP bound at the active site.[16–18] The structure of yeast PNPOx has been determined to 2.7 Å (RCSB entry 1CI0). Currently, the protein data bank lists amino acid sequences for 15 PNPOx enzymes from various sources. There is considerable sequence homology between all of these enzymes, suggesting that they share a common fold and mechanism. The *E. coli* enzyme has been

Abbreviations used: PLP, pyridoxal 5′-phosphate; PMP, pyridoxamine 5′-phosphate; PNP, pyridoxine 5′-phosphate; PNPOx, pyridoxine phosphate oxidase; SHMT, serine hydroxymethyltransferase.

E-mail address of the corresponding author: msafo@hsc.vcu.edu

0022-2836/02/030385–13 $35.00/0

© 2002 Academic Press

shown to exist in an open structure in the absence of bound PLP,[17] and a partially closed structure with PLP bound.[18] During the oxidation of either PNP or PMP, a pair of electrons and a hydrogen atom are removed from the C4′ and the electrons transferred to a tightly bound FMN moiety, forming $FMNH_2$. The electrons are then transferred to oxygen, forming H_2O_2 and regenerating the tightly bound FMN. Studies with the rabbit liver enzyme showed that it lacked stereospecificity in the hydrogen atom removed from the prochiral C4′ of PMP.[15] There was nearly equal removal of either the *pro*R or *pro*S hydrogen atoms as judged by equal numbers of ^3H atoms appearing in the H_2O or PLP fractions when (4′R)-[^{3}H]PMP was used as substrate.

We have determined a new crystal structure form of PNPOx with bound PLP in which residues 5-19, which were not seen in previous structures, are shown to form a lid on the active site. In this new structure, we see that Arg14 and Tyr17 both interact with the bound PLP at the active site and could potentially be important either in binding affinity or the mechanism of electron transfer. Kinetic constants were determined for several site mutants involved in PLP binding and the effect of these mutations on the stereochemistry of hydrogen removal from C4′ of PMP was determined.

Results

Structural properties of the monoclinic crystal form of PNPOx in complex with PLP

A monoclinic crystal form of PNPOx in complex with PLP diffracts to 2.07 Å resolution, although the crystals are small and have maximal size of about 0.03 mm × 0.03 mm × 0.8 mm. Suitable crystals for data collection are obtained after 6 to 12 months. The crystals belong to the space group $C2$ with unit cell constants $a = 83.36$ Å, $b = 52.24$ Å, $c = 53.91$ Å, $\beta = 101.45°$ and with one monomer per asymmetric unit. We were unable to obtain a monoclinic crystal form without co-crystallizing with PLP.

The secondary structure assignment and overall topology of the monoclinic crystal structure are identical with the trigonal structure, which has been determined with and without bound PLP.[17,18] Two monomers, which constitute the functional dimer, interact extensively along one-half of each monomer, as discussed.[17] Each monomeric subunit consists of two domains (1 and 2) folded into an eight-stranded β-sheet surrounded by five α-helical structures. The larger domain 1 is formed by the β-sheets β1-β5 and two of the five α-helices, α1 and α2. The smaller domain 2 is made up of the three remaining α-helices, α3, α4 and α5.

To compare the PNPOx structures, dimeric models of the trigonal and monoclinic crystals are superimposed using the LSQ procedures of O.[19] For the trigonal crystal, the model containing PLP is used, unless noted otherwise. The trigonal and monoclinic crystal structures are matched with a root-mean-square deviation of 0.51 Å for 396 C^α atoms, using residues 21-218 of the dimeric structure. If a more stringent criterion for LSQ-fitting of 1.0 Å is used, the root-mean-square deviation between the models is 0.37 Å for 364 C^α atoms. As shown in Figure 1, models from the trigonal and the monoclinic crystals fit with minimal deviations, including the FMN, PLP and phosphate groups. These non-protein molecules interact with PNPOx by the same repertoire in both crystals, except some additional bonds involving the PLP and the N-terminal residues in the monoclinic crystal. Refinement statistics for the monoclinic structure are recorded in Table 1. Asn208, the only residue found in the disallowed region of the Ramachandran plot, has glycine-like ϕ and ψ dihedral angles of 67° and −133°, respectively, for the second position in a type II′ turn.[20]

The monoclinic model shows a hitherto unseen structure of the N terminus (residues 5-19) (Figures 1 and 2). In the trigonal crystal, the first residue that could be identified was Gly20. Residues 8-13 constitute a short 3_{10} helix with the carbonyl oxygen atoms of Gln8, Gln9 and Ile10 hydrogen bonded to the nitrogen atoms of Ala11, His12 and Leu13, respectively. Residues 14-18 are in extended conformation, stretching over the active site. The NE and NH2 atoms of Arg14, and the OH atom of Tyr17 form hydrogen bonds with two phosphate oxygen atoms and the aldehyde oxygen atom of PLP, respectively. There is no strong conservation of Arg14 and Tyr17 in other PNPOx sequences, but the other enzymes do show in this extended region of the N terminus complete conservation of residues that can form hydrogen bonds. There are a number of other hydrogen bonds between this N-terminal segment with the rest of the PNPOx dimer, including a bifurcated

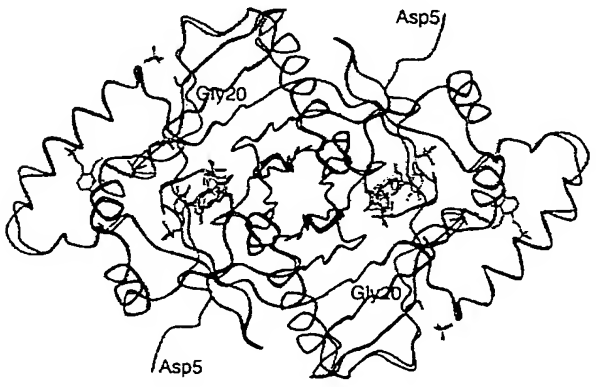

Figure 1. Least-squares superposition of monoclinic PNPOx dimer structure (red) with that of the trigonal PNPOx dimer structure (purple). The FMN, PLP and phosphate molecules of the monoclinic PNPOx structure are shown in magenta, while those of the trigonal structure are shown in green. The structures were superimposed as described in the text. The Figure was drawn using MOLSCRIPT[30] and Raster3D.[31]

Table 1. Data collection and refinement statistics of the PNPOx crystal

A. *Data collection statistics*		
Space group	C2 (b-unique)	
Unit cell dimensions		
a, *b*, *c* (Å)	83.36, 52.24, 53.91	
β (deg.)	101.45	
Resolution (Å)	40-2.07 (2.14-2.07)	
No. measurements	32,505	
No. unique reflections	13,510	
$I/\sigma I$	8.3 (2.1)	
Completeness (%)	96.6 (92.9)	
R_{merge} (%)[a]	7.7 (26.4)	
B. *Structure refinement*		
Resolution limit (Å)	40-2.07 (2.15-2.07)	
No. reflections	13,510 (1403)	
R-factor for 95% working data set	0.178 (0.293)	
R_{free} for 5% test data set	0.230 (0.349)	
rmsd from standard geometry		
Bond (Å)	0.010	
Angles (deg.)	1.54	
Dihedral (deg.)	22.9	
Improper (deg.)	2.45	
Average *B*-values (Å²)		
All 2094 non-hydrogen atoms	27.8	
The 856 backbone atoms	25.1	
The 919 sidechain atoms	27.2	
The 31 FMN atoms	18.2	
The 16 PLP atoms	21.5	
The 5 phosphate atoms	24.9	
The 267 water molecules	40.2	
Ramachandran plot (%)		
Most favored region	91.1	
Additional allowed region	6.8	
Generously allowed	1.6	
Disallowed region	0.5	
Estimated coordinate error (Å)	*R*-factor	R_{free}
By Luzzati plot	0.22	0.29
By SigmaA plot	0.30	0.35

Numbers in parentheses refer to the outermost resolution bin.

[a] $R_{merge} = \Sigma(\langle I \rangle - I)/\Sigma I$.

salt-bridge between the side-chains of Arg15 and Asp49 of the other subunit. The side-chains of Ile10 and Leu13 in the 3_{10} helix are involved in hydrophobic interaction with a non-polar patch formed by Leu39, Cys43, Pro50, Thr51, Leu71 and Tyr74 in the other subunit.

Crystal packing

The specific volumes, or Matthews coefficients,[21] of the trigonal and monoclinic crystals are 3.01 and 2.38 Å³/Da, respectively. This reduced volume in the monoclinic crystal cannot be explained by the extensive interactions between subunits within a dimer, because they are virtually identical for both crystal forms, which involve about 2600 Å² surface area on each subunit (see Safo *et al.*[17] for a description of these contacts). Rather, the reduced specific volume in the monoclinic crystal is due to differences in dimer packing. In the trigonal crystal, each dimer is in contact with four neighbours, related by the 3_1 screw symmetry axis inside the unit cell body, *via* identical interfaces. Not including water molecules, the interface buries 639 Å² and 636 Å² surface areas on the two dimers in contact. The total crystal contact area is 2550 Å² per dimer, accounting for about 15% of the dimer surface (17,930 Å²). This is within the typical range of 1100-4400 Å² per molecule[22] for crystal contact areas. In one of the dimers, only one subunit is involved (14 residues), while in the other both subunits are involved (11 and 2 residues). Table 2 lists specific bonds between residues in direct contact in the dimer. In addition, there are at least 31 interface water molecules.

In the monoclinic crystal, each dimer is in contact with six neighbours, four related by the C-centering symmetry and two by unit translation along the *c*-axis. The first type of interface buries 710 Å² and 694 Å² areas on the opposing dimers and involves 17 and 16 residues, respectively. The second type buries 494 Å² and involves 14 residues on each dimer. The total buried area is 3796 Å² per dimer, or about 21% of the dimer surface (18,293 Å²), indicating more involved molecular packing than the trigonal crystal form. Some specific bonds are listed in Table 2. There are at least 36 and 16 water molecules near the two interfaces. Among the 16 residues of the second dimer of the first interface, ten are from one subunit and the remaining six are from another subunit. The latter encompass the N terminus, which is sandwiched between two dimers as shown in Figure 3. This explains why these residues are seen only in the monoclinic crystal. In addition, the second interface contains a hydrophobic patch involving the dyad-related side-chains of Leu27, Ala29 and Ile213. The peptide N and O atoms of Trp211 also form two water-bridged hydrogen bonds across the dyad axis.

Table 2. Specific bonds at lattice contacts of PNPOx crystals

Residue 1	Atom 1	Residue 2	Atom 2	Distance (Å)
A. *Trigonal: Residues 1 and 2 belong to dimers related by* x, y, z *and* −y, x−y+1, z+1/3				
Glu94	OE1	Arg23	NH1	2.97
Glu94	OE2	Arg23	NH2	2.70
Thr123	OG1	Ile213	O	2.59
Ser176	O	Arg24	NE	3.00
Ser176	OG	Leu27	O	2.64
B. *Monoclinic 1: Residues 1 and 2 belong to dimers related by* x, y, z *and* x−1/2, y−1/2, z				
Glu94	OE1	Leu7*	N	2.87
Glu94	OE2	His12*	NE2	2.71
Lys117	NZ	Gln169	O	3.35
Glu119	OE1	Arg135	N	2.70
Ser176	OG	Gln9*	OE1	2.84
Arg206	O	Gln169	NE2	3.00
Asn208	N	Gln168	OE1	3.02
Asn208	ND2	Gln165	OE1	2.98
Arg206	O	Gln168	NE2	3.24
C. *Monoclinic 2: Residues 1 and 2 belong to dimers related by* x, y, z *and* x, y, z+1				
Leu27	O	Ala29	N	2.63
Ala29	N	Leu27	O	2.63

*Residues belonging to different subunits of the symmetry-related dimer.

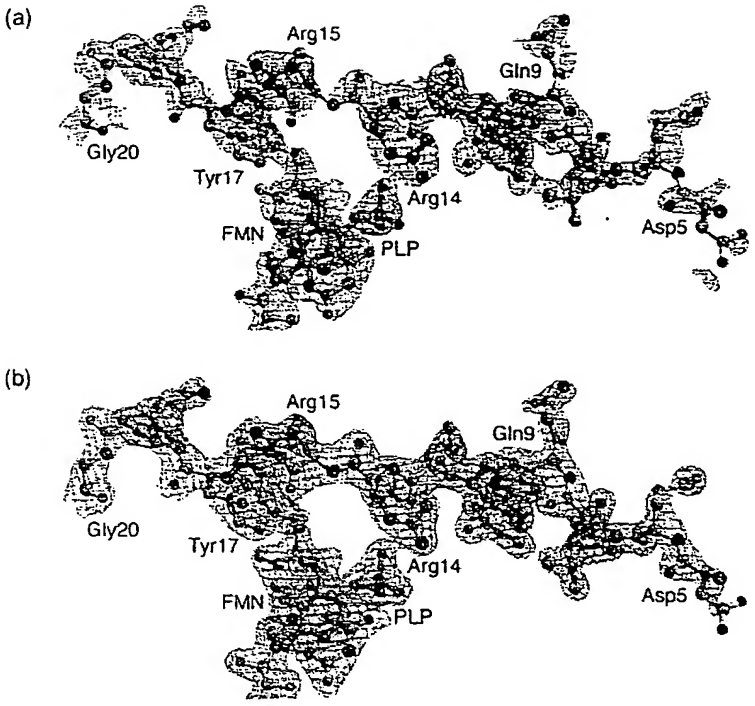

Figure 2. Difference Fourier ($2F_o - F_c$) maps of the monoclinic PNPOx crystal for the N-terminal region. The maps were calculated at 2.07 Å resolution using all reflections and phase angles of (a) the initial protein model after molecular replacement search and (b) the final model refined by CNS. Maps were contoured at the 1.0 σ level and superimposed with the refined model. The polypeptide sequence shown is DELQQIAHLRREYTKG. The associated FMN and PLP molecules are also shown. The Figures were produced using Bobscript[32] and Raster3D.[31]

We were unable to obtain a monoclinic crystal form without co-crystallizing with PLP. The reason could be due to the fact that the monoclinic structure represents a completely closed form of PNPOx, in which the N-terminal segment makes a number of interactions with the substrate PLP. Additionally, the N terminus is extensively involved in lattice contacts. Without bound PLP, the N terminus would remain flexible and disordered in solution. Therefore, it could not be packed properly into the monoclinic lattice due to lack of stabilizing inter-dimer contacts at the molecular interface. Most likely, it is the combination of these interactions involving the lattice and the bound PLP that have led to the stabilization of the N terminus and this explains why these residues are seen in the monoclinic crystal. In contrast, the N terminus in the trigonal crystal faces the bulk solvent and lacks the lattice contacts observed in the monoclinic crystal. This has therefore led to its disorder, even though the trigonal crystal also binds PLP.

Active-site interactions

We have previously discussed the active site in both open and partially closed forms.[17,18] In the native trigonal PNPOx without any bound PLP, the active site is open, while in the trigonal crystal with PLP bound the C terminus of helix α3, helix α4, and the loop located between these two helices (residues 129 - 140) have shifted 1.4 Å and rotated 2.7° toward the active-site cavity. This tertiary movement enables the residues Tyr129, Arg133 and Ser137 to come closer and make interactions with the PLP phosphate moiety. In addition, the flexible turn located between the strands S6 and S7 (residues 193-199), has shifted and rotated about 2.4 Å and 9.4°, toward the active site, and allows closer hydrogen bond interaction between PLP and the residues His199 and Arg197.

In the monoclinic crystal, the FMN molecule and the disposition of protein side-chains about it remain identical as in the trigonal crystal. The substrate PLP molecule occupies the same position in the active site and has essentially unaltered conformation in both crystals. In addition the two crystals show similar interactions between the protein and the bound PLP, with only a few rearrangements of some active-site residues. However, there are additional N-terminal residues that contribute to interaction with the PLP in the monoclinic crystal. The specific interactions between the PLP and the monoclinic crystal protein residues at the active site are shown in Figure 4. Three hydrogen bonds are conserved, between the OP1, OP2, and O3' atoms of PLP and the NZ (2.7 Å), OH (2.5 Å), and NE2 (2.6 Å) atoms of Lys72, Tyr129 and His199*, respectively. Interestingly, the guanidinium groups of both Arg133 and Arg197* are flipped over, resulting in NE and NH1 making two proper hydrogen bonds with the PLP phosphate moiety of 2.6 Å and 2.8 Å for Arg133 and 2.9 Å and 3.3 Å for Arg197*. In the trigonal crystal structure, only the NH1 atoms from the two residues are in hydrogen bond contact with the phosphate group. The side-chain of Arg197* also moves closer to the phosphate group, probably assisted in part by the hydrogen bonding of its NH2 atom to the backbone oxygen atom of Arg15* (not shown in Figure 4).

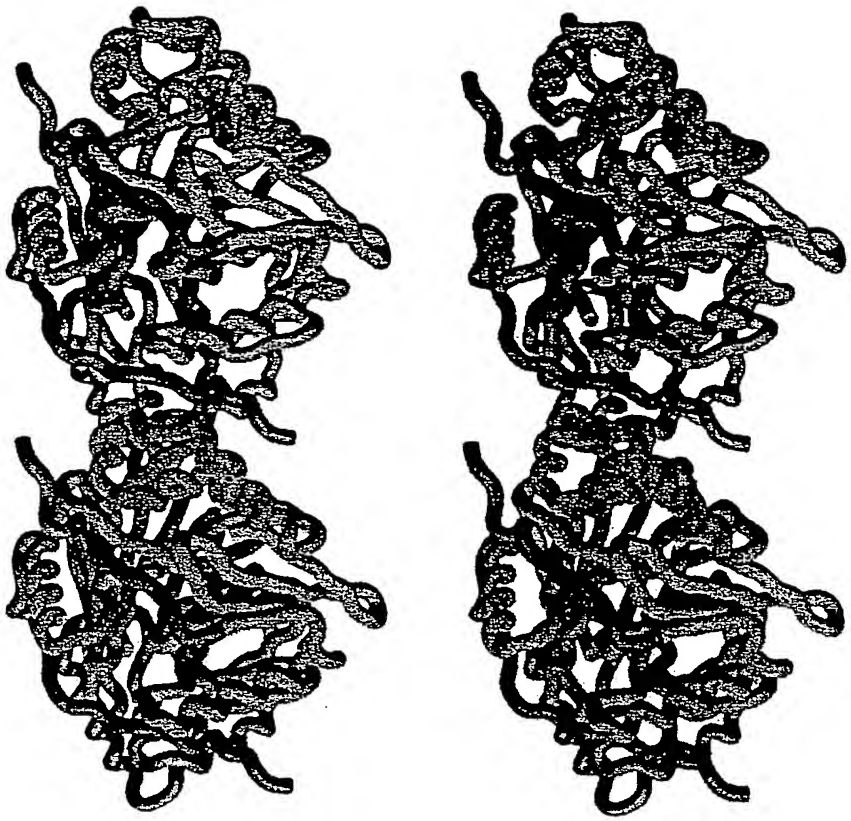

Figure 3. Stereo drawing of two neighbouring PNPOx dimers related by C-centering symmetry operation ($x + 1/2$, $y + 1/2$, z) in the monoclinic crystal. The polypeptide chains are coloured cyan and magenta in one dimer, and green and blue in the other. The sandwiched N-terminal segment between the two dimers is shown in red. The extensive interactions with the neighbouring molecule at the crystal contact interface rendered more stability and less mobility of the N terminus, and thus allows it to be observed in the monoclinic crystal. This Figure was produced using GRASP.[33]

As described previously, the newly identified N-terminal segment (residues 5-19) in the monoclinic crystal stretches over the active-site cavity entrance of the adjoining monomer to completely sequester the PLP, with the NE and NH2 atoms of Arg14* forming two unique hydrogen bonds with the PLP phosphate group of 3.0 Å and 3.3 Å, respectively. In addition, the Tyr17* hydroxyl group also makes a short hydrogen bond (2.8 Å) with the aldehyde oxygen atom of PLP. Thus, while the trigonal complex has a partially closed active site, that of the monoclinic complex is completely closed.

Kinetic properties of active-site residues

As shown in Figure 4, several residues that could be potentially important in binding and catalysis can be identified. These residues were mutated individually to test for their role in the PNPOx mechanism. We have made the following mutant PNPOx forms; H199A, H199N, D49A, Y17F, R14E, R14M, R197M and R197E. The K_m and k_{cat} values, for each of these mutants are shown in Table 3. Except for H199N, all mutations have increased K_m values, with H199A, R197 M and R197E showing greatly decreased affinity for PNP. Only R197E shows a large decrease in catalytic activity.

His199 forms a hydrogen bond to O3' of the bound product PLP (Figure 4). This residue is conserved in all 15 currently known PNPOx sequences. Replacing His199 with another hydrogen bond donor (Asn199) results in no change in K_m, but about a fourfold decrease in k_{cat} (Table 3). However, removing this hydrogen bond in the H199A mutant results in a 233-fold decrease in affinity but with no effect on k_{cat}. This suggests that a hydrogen bond is critical for binding, but

Table 3. Kinetic constants for active site mutants of *E. coli* PNPOx

Enzyme	K_m (μM)	k_{cat} (s^{-1})
Wild-type	0.30	0.13
H199A	70	0.14
H199N	0.30	0.03
D49A	1.0	0.06
Y17F	1.0	0.60
R14E	2.0	0.16
R14M	2.6	0.14
R197M	90	0.03
R197E	2400	0.008

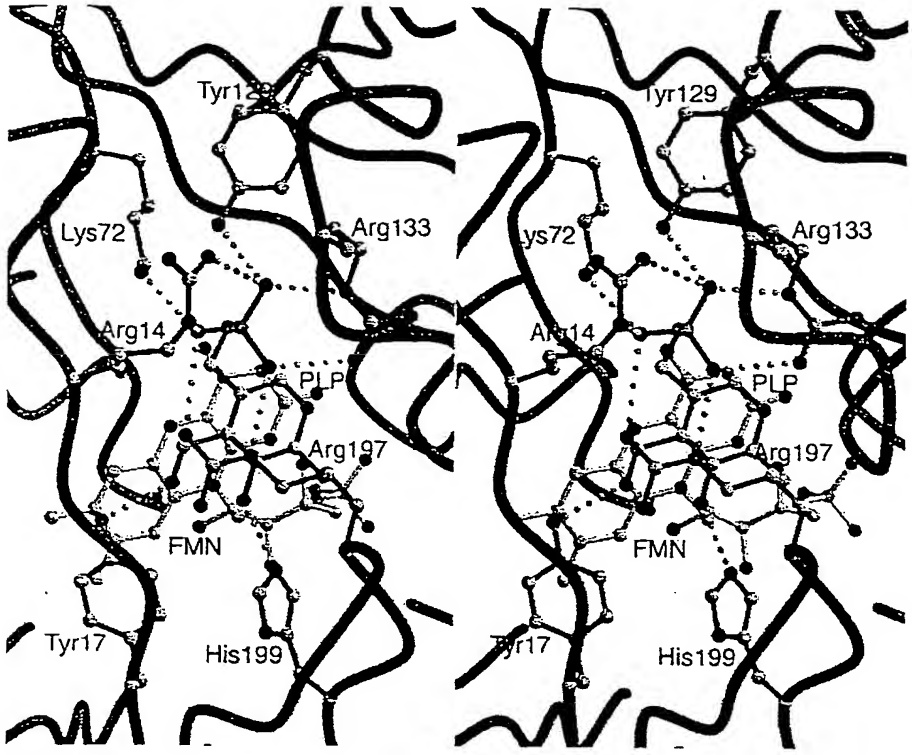

Figure 4. Stereoview of the active site of monoclinic PNPOx showing the FMN cofactor (yellow), PLP ligand (green) and associated protein residues. Hydrogen bond and/or salt-bridge interactions are shown between PLP and protein residues from monomer A (cyan) and monomer B (magenta). Atoms are shown in stick representation, with oxygen and nitrogen atoms coloured red and blue, respectively. The Figure was drawn using MOLSCRIPT[30] and Raster3D.[31]

that the basic property of His199 is not important for catalytic activity. The His199 imidazole side-chain is hydrogen bonded to the carboxylate side-chain of Asp49 (not shown in Figure 4). Removing this hydrogen bonding capability in the D49A mutant increase the K_m value by a factor of 3 and decreases k_{cat} by a factor of 2, suggesting that Asp49 plays a minor role in binding and catalytic activity. Residue 49 is conserved as either Asp or Glu in 12 of the currently known 15 sequences for PNPOx.

Tyr17 and Arg14 are a part of the N-terminal lid that covers the active site. The hydroxyl group of Tyr17 forms a 2.8 Å hydrogen bond to the C4′ oxygen atom of PLP (Figure 4). Removing the hydrogen bonding property of Tyr17 in the Y17F mutant results in a threefold increase in K_m, but a 4.6-fold increase in k_{cat}. Since the mechanism of PNPOx is not yet fully understood, we cannot explain the increase in the k_{cat} value, but it might mean that lifting the amino-terminal lid allowing product release may be at least partially rate-determining. Tyr17 is conserved in only six of the 15 structures, but in eight of the remaining nine sequences it is replaced by a group that can form a hydrogen bond with PLP. The guanidinium group of Arg14 forms two hydrogen bonds of 3.0 and 3.3 Å to two oxygen atoms of the phosphate moiety of PLP. Changing the positive charge to a negative charge in the R14E mutant increases K_m by about sixfold, but has no effect on k_{cat}. Removing the positive charge in the R14 M mutant reduces affinity by eightfold, but again has no effect on k_{cat}. Arg14 is conserved in only six of the 15 members of this family.

Arg197 lies above the plane of the PLP ring and its guanidinium group forms a bifurcated set of hydrogen bonds with two oxygen atoms of the phosphate group of PLP of 2.9 Å and 3.3 Å (Figure 4). However, the guanidinium group also lies 3.6 Å above the aldehyde moiety of PLP, suggesting that this residue may be important for binding of the substrate PNP and involved in chemistry by organizing adjacent residues and bound water molecules. These conclusions are supported both by the effects of mutations on this residue and its conservation in all 15 members of the PNPOx family. Changing the positive charge of Arg197 to a neutral side-chain in R197 M results in a 300-fold increase in K_m and a fourfold decrease in k_{cat}. In the R197E mutant, K_m is increased 8000-fold and k_{cat} is decreased about 16-fold.

Stereochemistry of hydrogen removal from C4′ of PNP

Scheme 1 shows the strategy used to determine the stereochemistry of hydrogen removal from C4′

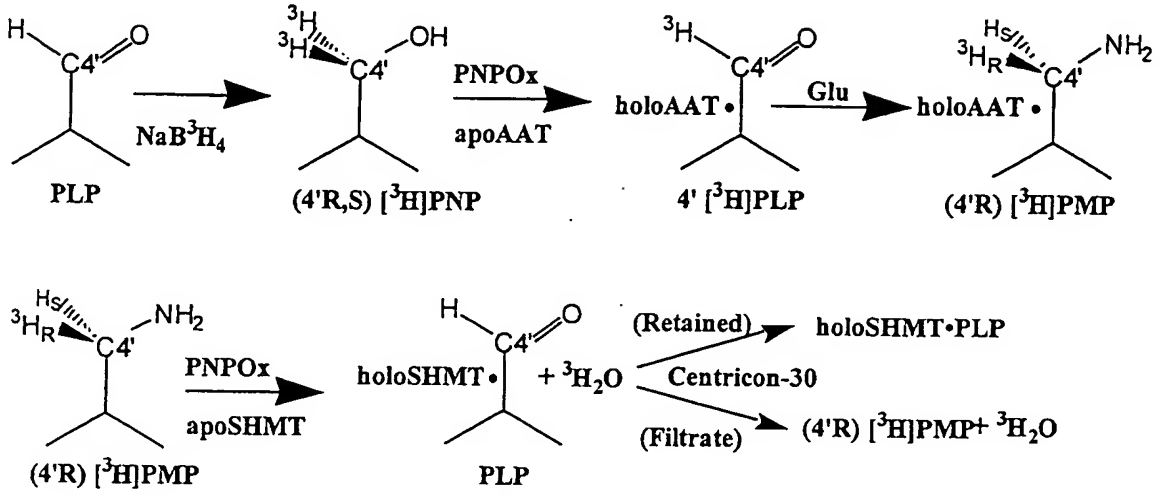

Scheme 1. Reactions used to determine stereospecificity of PNPOx. Upper line, reactions used to make (4'R)-[^{3}H]PMP. Bottom line, reactions used for determining stereospecificity of PNPOx.

of PMP. This is based in large part on the same method used to determine the stereochemistry of rabbit liver PNPOx.[15] The key to this procedure is the preparation of (4'R)-[^{3}H]PMP using the known stereochemistry of aspartate aminotransferase in converting PLP to PMP.[23] The aspartate aminotransferase forms PMP stereospecifically and it serves as a convenient purification method allowing the separation of the bound PMP from other reactants by size-exclusion chromatography. The PMP is freed at neutral pH by ethanol-denaturation of aspartate aminotransferase.

The oxidation of (4'R)-[^{3}H]PMP transfers one of the C4' hydrogen atoms to H_2O and leaves the other hydrogen atom on the product PLP (Scheme 1, bottom line). PLP binds to an excess of apoSHMT, which again provides a convenient purification method because of the large size relative to unreacted (4'R)-[^{3}H]PMP and H_2O. We used a filtration device to separate the product PLP from the other two potentially radioactive components. A blank sample in which PNPOx was omitted showed that 99% of the counts passed through the filter (Table 4). However, when the sample was dried, 90% of these counts remained, showing that the counts were attributable to the unreacted substrate (4'R)-[^{3}H]PMP. The observation that less than 100% of the counts remained after drying is most likely a result of experimental error due to small volume determinations or minor radioactive contaminants in the (4'R)-[^{3}H]PMP sample.

Using wild-type PNPOx and (4'R)-[^{3}H]PMP as substrate, we found 99% of the radioactivity in the filtrate. After drying, only 7% of the counts remained in the filtrate, suggesting that about 93% of the counts were originally present as ^3H_2O (Table 4). This means that in the oxidation of (4'R)-[^{3}H]PMP the *pro*R hydrogen atom on C4' is removed and the *pro*S hydrogen atom remains with PLP. The non-volatile counts in the Microcon-30 flow-through fraction most likely are attributable to unreacted (4'R)-[^{3}H]PMP.

The stereospecificity was determined for each of the mutant enzymes. Except for R197 M, all mutant PNPOx reactions result in transfer of the *pro*R hydrogen atom of PMP to H_2O. With the R197 M PNPOx, 64% of the counts were in the fil-

Table 4. Stereochemistry of PNPOx oxidation of (4R)-[^{3}H]PMP to PLP

Enzyme	cpm in Micron-30 flow-through	cpm in the Micron-30 retained fraction	cpm in the dried flow-through fraction
Blank	16,600 (99)[a]	180 (1)	15,000 (90)
Wild-type	17,000 (99)	160 (1)	1400 (7)
H199N	15,100 (96)	600 (4)	650 (41)
D49A	17,000 (96)	900 (5)	600 (4)
Y17F	16,700 (99)	130 (1)	1300 (8)
R14E	17,400 (99)	135 (1)	1000 (6)
R14 M	17,200 (99)	100 (1)	1200 (7)
R197 M	11,700 (64)	6650 (36)	10,100 (86)

Each reported value is the average of two separate experiments with the variation in counts never being greater than ±1%. The values in parentheses are percentage of total counts.

[a] The total counts varied slightly between experiments, but was always in the range of 16,500 to 17,500 cpm.

trate and 36% were located in the holoSHMT fraction containing the product PLP. Of the counts in the flow-through fraction, 86% were not volatile, suggesting that there was less than 50% conversion of the PMP to PLP in this overnight incubation. However, the 6650 counts in the SHMT fraction shows that as much as 80% of the PMP that was converted to PLP came by removal of the *pro*S hydrogen atom on (4'R)-[^{3}H]PMP. This suggests that in this mutant there is significant loss of stereospecificity. R197E and H199A PNPOx have either high K_m or low k_{cat} values, resulting in insufficient PLP product being formed during the incubation to determine the location of the ^{3}H accurately.

Discussion

Studies on rabbit liver PNPOx showed that in the oxidation of PMP the enzyme lacks stereospecificity on removing the hydrogen atom from C4'.[15] As noted by the authors of the rabbit liver PNPOx study, there are two possible mechanisms for oxidizing the C4' alcohol or amine group to an aldehyde by a two-electron transfer. (There is no evidence for oxidation by two one-electron transfers to FMN). One mechanism is the transfer of a hydride ion from PNP to FMN, leaving an electron-deficient C4'. The proposed hydride ion transfer would generate a buildup of positive charge at C4', which could be resonance-stabilized by the electron pairs on O3' as shown in Scheme 2A. The

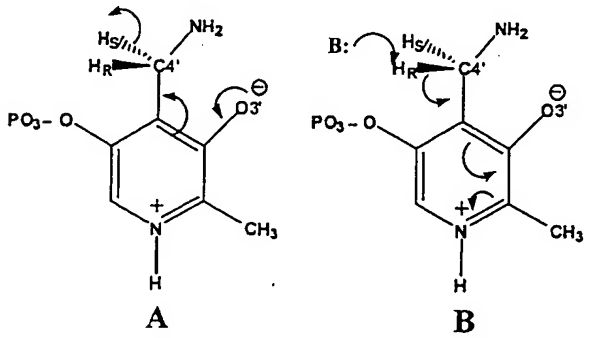

Scheme 2. Description of two possible mechanisms for the transfer of electrons from the substrate C4' to FMN. The FMN ring is in front of the PMP ring to correspond to the structure observed in the monoclinic crystal. (a) Possible mode of resonance stabilization during a hydride ion transfer of C4' H_R of PMP to FMN. (b) Possible mode of resonance stabilization during removal of a proton from C4' H_R of PMP to generate a C4' carbanion. The carbanion would then form a covalent adduct with FMN as a part of the electron transfer process.

other proposed mechanism for transferring a pair of electrons from the substrate to FMN is removing a proton from C4' of PNP (PMP), resulting in a C4' carbanion, which then forms a covalent adduct with FMN. A resonance-stabilized structure for the putative carbanion can also be proposed, as shown in Scheme 2B. The generation of the resonance-stabilized carbanion at C4' requires an active-site base to accept the proton from C4'. With either of these two proposed mechanisms it is difficult to envision a reaction without stereospecificity. With the *E. coli* PNPOx, we now see that the removal of the hydrogen atom from C4' is stereospecific.

With the monoclinic crystal structure of PNPOx in complex with PLP, as shown in Figure 4, we now have the structure of the closed form of the enzyme with all active-site residues in contact with the product PLP. With the folding of the N-terminal residues over the active site, two additional hydrogen bonds are formed between enzyme and substrate, and solvent is excluded during the conversion of PNP to PLP. Knowing the stereospecificity of the enzyme should provide a clear picture of the mechanistic pathway for PNPOx. In the substrate complex (PNP or PMP), C4' is tetrahedral and the lowest energy for the hydrogen atom that is removed will be perpendicular to the plain of the pyridine ring. In the hydride ion transfer mechanism, the hydrogen atom will be between the PNP and FMN rings (in Scheme 2A and B, FMN is in front of PMP). In the carbanion mechanism, the proton that is removed from C4' will be on the opposite side of the pyridine ring and away from the FMN ring.

Our results show that the labeled hydrogen atom of (4'R)-[^{3}H]PMP is removed during oxidation by PNPOx (Table 4). This finding supports the hydride ion transfer mechanism (Scheme 2A). The structure shown in Figure 4 has C4' of PLP located directly above N5 of FMN. The distance of 3.3 Å between C4' of PLP and N5 of FMN is optimal for hydride transfer. The mechanism shown in Scheme 2B requires a base to be located near H_R of C4', which would be pointing on the opposite side of the PMP ring as discussed above. There are only two residues near C4' of the bound PLP that could be the putative base. These are His199* and Tyr17* (Figure 4). When these two residues are changed to non-basic residues, the enzyme retains considerable catalytic activity, showing that neither can be the proton acceptor required by the mechanism shown in Scheme 2B (Table 3). Also, neither are in the correct position to accept the *pro*R hydrogen atom from C4' of PNP. There is a conserved water molecule located near the C4' hydroxyl group and the guanidinium group of Arg197*. It makes hydrogen bonds with four atoms; Arg197* NH1 (3.2 Å), Arg15* N (3.0 Å), Tyr17* OH (2.7 Å), and another water molecule (3.0 Å). Even though this water molecule has a very low *B*-factor (21 Å^2, compared to 40 Å^2 for the average water molecule) and is also 2.9 Å from H_R of PMP when it is oriented as shown in Scheme 2B, it is unlikely to be the putative base. There are several reasons for this conclusion. First, there is no additional valence electron available for bonding to C4' H_R. Also, changing Try17* to a non-hydrogen bonding Phe17* increases k_{cat} by 4.6-fold. Removing a

hydrogen bond from this water molecule should make it a weaker base and result in a decrease in k_{cat}. In the R197M mutant, k_{cat} is reduced only four-fold. A greater effect on removing a hydrogen bond donor and positive charge would be expected if this water molecule was the catalytic base. In none of our structures with PLP bound at the active site do we see any covalent bond between C4′ of the PLP and N5 of FMN, which would be an intermediate formed in a carbanion mechanism. But most important of all in eliminating the carbanion mechanism is the location of the aldehyde group of the product PLP. As shown in Scheme 2B, the amino group lies in a position that would put the product aldehyde oxygen atom on the side of the ring toward the phosphate residue and not O3′. Both the monoclinic and trigonal crystal structures show that in the PLP complex the aldehyde oxygen atom lies in the plane on the O3′ side of the ring.

This leaves unanswered why the rabbit PNPOx was found to lack stereospecificity in removing the hydrogen atom from C4′ of PMP.[15] The structure shown in Figure 4 is for the product PLP bound at the active site. C4′ is a planar trigonal sp^2 hybrid carbon atom in PLP. As noted above for the substrates PNP and PMP, C4′ has tetrahedral sp^3 hybridization. In Figure 5(a) is shown the active-site structure modeled for PNP or PMP binding at the active site and with 4C′ H_R both perpendicular and between the pyridine ring of the substrate(s) and the FMN ring system for optimum geometry of hydride ion transfer. In this model, the closest hydrogen bond distance of the OH or NH_2 group on C4′ to Tyr17* and Arg197* are 2.9 Å and 2.8 Å, respectively. The conserved water molecule is about 3.6 Å distant. If you rotate the bond between C4 and C4′ so that $4'H_S$ is now poised for transfer to FMN, the C4′ OH or NH_2 are now 3.6 Å and 2.8 Å from Tyr17* and Arg197* and 2.7 Å from the water molecule (Figure 5(b)). Since this is a model, the distances of the C4′ OH to the water molecule, Tyr17* and Arg197* are not so different that we can eliminate the possibility that the substrates PNP and PMP may be able to bind in either conformation, giving non-specific transfer of the *pro* chiral hydrogen atoms to FMN. In the conformation shown in Figure 5(b), the interaction of the OH or NH_2 group attached to C4′ with O3′ of the substrate ring is lost, which would argue against this conformation. This juxtaposition of the OH group of PNP or NH_2 group of PMP and the guanidinium group of Arg197* may determine why in *E. coli* PNPOx it is the structure corresponding to Figure 5(a) that is bound at the active site. In human and rat PNPOx sequences, Tyr17 is replaced by Asp. This change from a neutral to a negatively charged side-group may significantly alter how this residue interacts with the substrate and the location of Arg197*. The sequence of rabbit PNPOx is not known but may have a substitution for Tyr17* giving a slightly different set of interactions at the active site. This might permit both orientations shown in Figure 5 to be populated, thus resulting in a loss of stereochemistry in the hydrogen atom removed from C4′ of PMP.

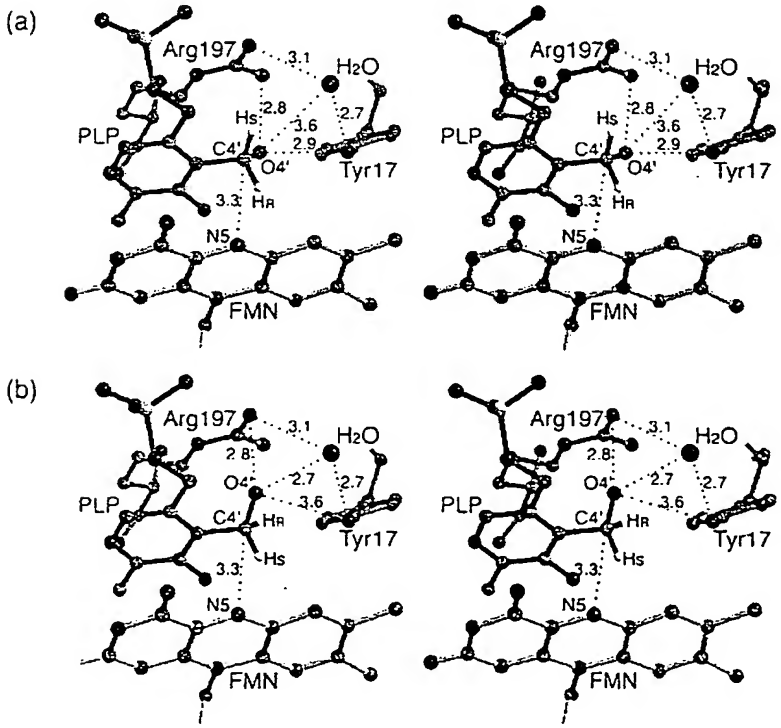

Figure 5. Model of PNP in the active site of monoclinic PNPOx showing interactions with C4′ as a tetrahedral carbon atom with either 4′ H_R or H_S pointed perpendicular and lying between the pyridine ring of PNP and N5 of FMN. (a) Model with C4′ H_R in position for a hydride transfer to FMN. (b) Model with C4′ H_S in position for a hydride transfer to FMN. The Figures were drawn using MOLSCRIPT[30] and Raster3D.[31]

We mutated Arg197 to Glu or Met to test its role in binding and stereochemistry. As recorded in Table 3, the affinity of PNP for both mutants has been decreased greatly. We attempted to determine the stereospecificity of both the R197E and R197M mutant enzymes, but this was not possible for the R197E mutant because of its greatly reduced affinity and catalytic activity. However, for the R197M mutant PNPOx, about 50% of the original 17,000 counts have been converted to the products PLP attached to holoSHMT and H_2O in the filtrate (6650 cpm in the retained fraction + 1600 cpm lost during drying of the filtrate, Table 4). Of these counts in the two products, about 80% appears in holoSHMT, showing that the R197 M mutant has lost significant stereochemical control and transfers the *pro*S hydrogen atom on C4' about 80% of the time. This suggests that Arg197* plays a significant role in binding of the substrate for optimum transfer of electrons to FMN.

Materials and Methods

Materials

PMP, PLP, PN, and PM were obtained from Sigma Chemical Co., St. Louis, MO. All buffer solutions were made of the purest components available. *E. coli* aspartate aminotransferase was purified from cell extracts of an over-expressing clone, kindly provided by Dr Roberto Contestabile, University of Rome.[24] *E. coli* PNPOx and rabbit liver cytosolic SHMT were purified from *E. coli* clones as described.[7,25] 4'-[^{3}H]PNP and 4'-[^{3}H]PLP were synthesized from unlabeled PLP and NaB[^{3}H]$_4$ (Amersham Life Science Inc., Arlington Heights, IL) as described.[26]

The apoSHMT was prepared by using L-cysteine to trap the PLP as a thiazolidine complex. L-Cysteine (10 mM) was added to 20 mg of purified SHMT in 100 mM potassium phosphate (pH 6.8), 25% saturated with ammonium sulfate. This solution was added to a 1 cm × 5 cm phenyl-Sepharose column equilibrated with the same L-cysteine/ammonium sulfate-containing buffer. The enzyme binds tightly and continued washing with this buffer results in removal of the bound PLP, leaving apoSHMT bound to the column. After all PLP has been removed, as evidenced by the lack of 330 nm absorbing material in the eluate, the apoSHMT is eluted with 10 mM potassium phosphate (pH 7.3), 1 mM dithiothreitol. The apoSHMT is concentrated and dialyzed against the eluting buffer.

Preparation of PNPOx site mutants

All mutant forms of PNPOx were made on the wild-type construct pET22::PNPOx[7] using the QuickChange™ Site-Directed Mutagenesis Kit from Stratagene (La Jolla, CA). Oligonucleotides were synthesized by Integrated DNA Technologies, Inc., (Coralville, IA). *E. coli* MDS00 (W3110 *lacI*169 *tna*2 *sup*^{0} Δ*pdxH*::Ω(Cm^r) (DE3)), used for expression of the mutant forms of PNPOx, were generated from *E. coli* strain TX2768 through a λDE3 Lysogenization Kit (Novagen, Madison, WI). For protein expression, bacterial cells were grown for 15 hours at 37 °C in 1.5 × LB medium without isopropyl-β-thiogalactoside induction. Protein purification was as described.[7] About 100 mg of each pure mutant protein was obtained per liter of culture.

Preparation of apoaspartate aminotransferase

Holoaspartate aminotransferase (150 mg; PLP form) was incubated at room temperature for a few minutes in 5 ml of buffer A (100 mM potassium phosphate (pH 6.0), 0.2 mM EDTA, 1 mM dithiothreitol and 50 mM L-glutamate). After addition of solid ammonium sulfate to 25% saturation, the solution was loaded onto a phenyl-Sepharose column (1 cm × 10 cm) equilibrated with buffer A containing ammonium sulfate at 25% saturation. The protein binds to the column as a sharp yellow band. The glutamate converts the enzyme-bound PLP to PMP, which dissociates under the high-salt condition. The column is washed with buffer A until the yellow band disappears and all pyridoxamine 5'-phosphate is eluted, as determined by the lack of an absorbance band at 325 nm in the eluate. The apoaspartate aminotransferase is eluted by first adding 5 ml of buffer A lacking the glutamate. This is followed by washing the column with 20 mM potassium phosphate (pH 6.0), 0.2 mM EDTA, 1 mM dithiothreitol containing 15% propylene glycol. Fractions containing apoaspartate aminotransferase absorbing at 280 nm are pooled and dialyzed against this buffer (without propylene glycol) after which the protein is concentrated by means of a Centriplus-30 filter device (Amicon-Millipore). The apoaspartate aminotransferase is stored at −20 °C at a concentration of about 18 mg/ml.

Preparation of (4'R)-[^{3}H]PMP

The upper line of Scheme 1 shows the strategy for preparing (4'R)-[^{3}H]PMP. A solution containing 50 nmol of apoaspartate aminotransferase, 1 nmol of PNPOx, 35 nmol of 4'-[^{3}H]PNP in 500 μl of 20 mM potassium phosphate (pH 7.3), 20 mM L-glutamate, 1 mM dithiothreitol is incubated at 37 °C for one hour. During this incubation the 325 nm absorbance of PNP shifts to the 355 nm and 428 nm absorbance peaks of holoaspartate aminotransferase. The reaction mixture is concentrated, by centrifugation in a Centricon-30 filter, to 250 μl and loaded onto a P6-DG column (1 cm × 13 cm) previously equilibrated with 20 mM potassium phosphate (pH 7.2), 20 mM L-glutamate, 1 mM dithiothreitol and eluted with the same buffer. The glutamate shifts the equilibrium of holoaspartate aminotransferase from the PLP form to the PMP form with the formation of 2-oxoglutarate. As the enzyme progresses down the sizing column, the 2-oxoglutarate is separated from the enzyme blocking the reverse reaction, resulting in complete conversion from the PLP form to the PMP form of holoaspartate aminotransferase. Fractions of 0.5 ml are collected and those containing aspartate aminotransferase are pooled and concentrated by centrifugation in a Centricon-30 filter. The concentrated protein in the Centricon-30 filter is diluted with 1 ml of 20 mM potassium phosphate (pH 7.2), 1 mM dithiothreitol buffer and again concentrated. This washing is repeated three times to remove all of the L-glutamate. The holoaspartate aminotransferase solution is then made 30% (v/v) in ethanol and incubated at 60 °C for 30 minutes to denature the protein and to release (4'R)-[^{3}H]PMP. After cooling to 4 °C, the precipitated protein is removed by centrifugation at 14,000 rpm for five minutes in a microcentrifuge. A spectrum of the supernatant (total volume 400 μl) is taken

and 10 µl counted for tritium content. With this procedure, an average specific activity of about 14,000 cpm per nmol for (4'R)-[^{3}H]PMP is obtained, as determined by using a molar absorbtivity coefficient of 8300 cm^{-1} M^{-1} for PMP at 324 nm.

Determination of stereospecificity of PNPOx

The strategy for determining the stereospecificity of PNPOx is given in the second line of Scheme 1. The substrate (4'R)-[^{3}H]PMP is oxidized by PNPOx to PLP and the ^{3}H will be released either as H_2O or retained in the product PLP depending on the hydrogen removed from C4'. PLP that is generated during the PNPOx reaction is trapped by rabbit cytosolic apoSHMT forming the holo enzyme. The H_2O and holoSHMT fractions are then separated by filtration.

A solution containing 0.6 nmol of (4'R)-[^{3}H]PMP, 6 nmol of apoSHMT, 0.9 nmol of PNPOx in 600 µl of 20 mM potassium phosphate (pH 7.3), 1 mM dithiothreitol is incubated at 37 °C for two hours. Then another 6 nmol of apoSHMT is added and the reaction incubated for an additional 30 minutes, or until the 325 nm absorbance peak of PMP has shifted completely to the 428 nm absorbance peak of holoSHMT (an overnight incubation was performed for some mutant forms of PNPOx). The reaction mixture is concentrated by centrifugation in a Microcon-30 filter at 14,000 rpm for 15 minutes. After two 150 µl water rinses of the retained fraction, the filtrate solutions are combined and 200 µl counted for tritium content. The filtrate will contain the water, buffer, and any unreacted (4'R)-[^{3}H]PMP, while the fraction retained by the Microcon-30 membrane will contain the holoSHMT with the bound PLP. To determine if the counts in the filtrate are H_2O or residual (4'R)-[^{3}H]PMP, a 200 µl aliquot is dried by vacuum centrifugation and dissolved in 500 µl. This process is repeated three times. After the final drying, the remaining residue is dissolved in 200 µl of H_2O and counted to determine how much of the original radioactivity in the filtrate is not volatile, which is a measure of the unreacted (4'R)-[^{3}H]PMP.

The retentate of the Microcon-30 filter containing the PLP bound to SHMT is dissolved in 300 µl of 20 mM potassium phosphate (pH 7.3), 1 mM dithiothreitol and 70 µl counted for tritium content.

Assays and determination of kinetic constants

Determination of catalytic activity during purification is performed in a 1 cm cuvette with 50 mM Tris·HCl (pH 8.0), 1 mM dithiothreitol as the buffer at 37 °C.[26] (The kinetic constants do not change between pH 7.0, where the crystal structure was determined, and pH 8.0 for PNPOx.) The product PLP forms an aldimine with the Tris buffer that absorbs at 414 nm with a molar absorbtivity coefficient of 5900 cm^{-1} M^{-1}. When determining K_m and k_{cat} values, a 10 cm pathlength cell is used with 20 mM Tris (pH 8.5), 1 mM dithiothreitol. The PNP concentration is varied between 0.3 and two times the K_m value. Enough PNPOx is added to give a maximum rate of about $\Delta A_{414\ nm}$ of 0.1 per minute. K_m and k_{cat} values are determined from double reciprocal plots constructed with Sigma Plot. The concentration of PNPOx is determined from its absorbance at 278 nm as described.[7]

Crystallization and data collection

Crystallization and structure determination of PNPOx in a trigonal unit cell has been described.[16–18] A monoclinic crystal form, with a needle morphology, was grown with a 9.3 mg/ml SeMet derivative of the native protein solution in 100 mM potassium phosphate (pH 7.5), 5 mM 2-mercaptoethanol by the hanging-drop, vapor-diffusion method. The drop contained 3.0 µl of protein, 0.2 µl of 13 mM PLP and 3 µl of reservoir solution (1 M $(NH_4)_2SO_4$, 1.5% (v/v) dioxane, 0.1 M 2-[*N*-morpholino]ethanesulfonate/NaOH buffer, pH 7.0). The final molar ratio of protein to PLP is approximately 1:5. Crystals appear after three months and grow slowly to sizes suitable for X-ray data collection after six months.

Diffraction data sets were collected at 100 K using a Molecular Structure Corporation (MSC) X-Stream Cryogenic Crystal Cooler System (Molecular Structure Corporation, The Woodlands, TX, USA), an R-Axis II image plate detector equipped with OSMIC confocal mirrors and a Rigaku RU-200 X-ray generator operating at 50 kV and 100 mA. Prior to use in X-ray diffraction, the monoclinic crystals are first washed in a cryoprotectant solution containing 2.1 M $(NH_4)_2SO_4$, 4.2 mM PLP, 7.7% (v/v) glycerol and then transferred to a similar solution containing 14.2% glycerol. All data are processed using the BIOTEX software of MSC and the CCP4 suite.[27] Statistics for the data set used in the refinements are listed in Table 1.

Structure determination and refinement

The monoclinic crystal form of *E. coli* PNPOx was solved by molecular replacement methods using the program AMoRe of the CCP4 suite.[27] The monomeric trigonal crystal structure,[17,18] omitting all FMN, PLP, phosphate and water molecules was used to determine the structure of the monoclinic crystal form. Based on the solvent content of the unit cell (43%, v/v), we expected one monomer in the asymmetric unit. The cross-rotation function was calculated using normalized structure factors with data in the resolution range of 8.0 to 4.0 Å. One unique solution was observed with a correlation coefficient of 26.1. The translation function, using the space group C2 resulted in a correlation coefficient and *R*-factor of 54.5 and 39.4%, respectively.

Structure refinements were performed with the CNS program,[28] with overall anisotropic *B*-factor correction and a bulk solvent correction. A statistically random selection of 5% of the total reflection data was excluded from the refinement and used to calculate the free *R*-factor (R_{free}) as a monitor of model bias.[29] Rigid-body refinement of the molecular replacement model gave an *R*-value of 0.364 for the entire data set at 2.07 Å. In the initial $2F_o - F_c$ map, shown in Figure 2(a), there are densities for both FMN and PLP molecules at the active site. The N-terminal Gly20 did not have corresponding density and was deleted. However, densities in the nearby regions indicated a different N-terminal extension. All of these were first modelled as 78 water molecules. After one round of positional and simulated annealing refinement, a second $2F_o - F_c$ map was calculated. It clearly showed densities for amino acid residues 8-20, which were missing from our previous structures of PNPOx.[17,18] With all water molecules replaced by the N terminus residues 8-20, and addition of FMN and PLP, the model yielded *R* and R_{free} values of 0.258 and 0.295, respectively. Further refinement cycles included addition

of 267 water molecules and a phosphate ion, as well as extension of the N terminus to Asp5. A portion of the final $2F_o - F_c$ map is shown in Figure 2(b). Omit $2F_o - F_c$ and $F_o - F_c$ electron density maps were repeatedly used to inspect the structure for positional corrections. All model building and model corrections were carried out using the program O.[19] Refinement statistics are summarized in Table 1.

Protein Data Bank accession numbers

The atomic coordinate and structure factor sets for the monoclinic structure have been deposited in the RCSB Protein Data Bank with accession code 1jnw.

Acknowledgments

This work was supported by grants DK 55648 (to V.S.) and HL04367 (to M.K.S.) from the National Institutes of Health. M.L.D.S. was partly supported by a grant from Ministero Istruzione Università e Ricerca (MIUR).

References

1. Zhao, G. & Winkler, M. (2000). Kinetic limitation and cellular amount of pyridoxine (pyridoxamine) 5'-phosphate oxidase of *Escherichia coli* K-12. *J. Bacteriol.* **177**, 883-891.
2. Hill, R. E., Himmeldirk, K., Kennedy, I. A., Pauloski, R. M., Sayer, B. G., Wolf, E. & Spenser, I. D. (1996). The biogenetic anatomy of vitamin B_6. *J. Biol. Chem.* **271**, 30426-30435.
3. Choi, J-D., Bowers-Komro, D. M., Davis, M. D., Edmondson, D. E. & McCormick, D. B. (1983). Kinetic properties of pyridoxamine (pyridoxine)-5'-phosphate oxidase from rabbit liver. *J. Biol. Chem.* **258**, 840-845.
4. Kazarinoff, M. N. & McCormick, D. D. (1975). Rabbit liver pyridoxamine (pyridoxine) 5'-phosphate oxidase: purification and properties. *J. Biol. Chem.* **250**, 3436-3443.
5. Choi, S. Y., Churchich, J. E., Zaiden, E. & Kwok, F. (1987). Brain pyridoxine-5'-phosphate oxidase: modulation of its catalytic activity by reaction with pyridoxal 5'-phosphate and analogs. *J. Biol. Chem.* **262**, 12013-12017.
6. Churchich, J. E. (1984). Brain pyridoxine-5-phosphate oxidase: a dimeric enzyme containing one FMN site. *Eur. J. Biochem.* **138**, 327-332.
7. Di Salvo, M., Yang, E., Zhao, G., Winkler, M. E. & Schirch, V. (1998). Expression, purification, and characterization of recombinant *Escherichia coli* pyridoxine 5'-phosphate oxidase. *Protein Express. Purif.* **13**, 349-356.
8. Kazarinoff, M. N. & McCormick, D. B. (1973). N-(5'-phospho-4'-pyridoxyl) amines as substrates for pyridoxine (pyridoxamine) 5'-phophate oxidase. *Biochem. Biophys. Res. Commun.* **52**, 440-446.
9. Merrill, A. H., Horiike, K. & McCormick, D. G. (1978). Evidence for the regulation of pyridoxal 5'-phosphate formation in liver by pyridoxamine (pyridoxine) 5'-phosphate oxidase. *Biochem. Biophys. Res. Commun.* **83**, 984-990.
10. Kazarinoff, M. N. & McCormick, D. B. (1974). Specificity of pyridoxine (pyridoxamine) 5'-phosphate oxidase for flavin-phosphates. *Biochim. Biophys. Acta*, **359**, 282-287.
11. Horiike, K., Merrill, A. H., Jr & McCormick, D. B. (1979). Activation and inactivation of rabbit liver pyridoxamine (pyridoxine) 5'-phosphate oxidase activity by urea and other solutes. *Arch. Biochem. Biophys.* **195**, 325-335.
12. Horiike, K., Tsuge, H. & McCormick, D. B. (1979). Evidence for an essential hisdtidyl residue at the active site of pyridoxamine (pyridoxine)-5-phosphate oxidase from rabbit liver. *J. Biol. Chem.* **254**, 6638-6643.
13. Merrill, A. H., Jr, Korytnyk, W., Horiike, K. & McCormick, D. B. (1980). Spectroscopic studies of complexes between pyridoxamine (pyridoxine)-5-phosphate oxidase and pyridoxyl 5'-phosphate compounds differing at position 4'. *Biochim. Biophys. Acta*, **626**, 57-63.
14. Choi, J.-D. & McCormick, D. B. (1981). Roles of arginyl residues in pyridoxamine-5'-phosphate oxidase from rabbit liver. *Biochemistry*, **20**, 5722-5728.
15. Bowers-Komro, D. & McCormick, D. B. (1985). Pyridoxamine-5'-phosphate oxidase exhibits no specificity in prochiral hydrogen abstraction from substrate. *J. Biol. Chem.* **260**, 9580-9582.
16. Musayev, F. N., Safo, M. K., di Salvo, M. L., Schirch, V. & Abraham, D. J. (1999). Crystallization and preliminary X-ray crystallographic analysis of pyridoxine 5'-phosphate oxidase complexed with flavin mononucleotide. *J. Struct. Biol.* **137**, 88-91.
17. Safo, M. K., Mathews, I., Musayev, F. N., di Salvo, M. L., Thiel, M. L., Abraham, D. J. & Schirch, V. (2000). X-ray structure of *Escherichia coli* pyridoxine 5'-phosphate oxidase complexed with FMN at 1.8 Å resolution. *Structure*, **8**, 751-762.
18. Safo, M. K., Musayev, F. N., di Salvo, M. L., & Schirch, V. (2001). X-ray structure of *Escherichia coli* pyridoxine 5'-phosphate oxidase complexed with pyridoxal 5'-phosphate at 2.0 Å resolution. *J. Mol. Biol.* **310**, 817-826.
19. Jones, T. A., Zou, J.-Y., Cowan, S. W. & Kjeldgaard, M. (1991). Improved methods for building protein models in electron density maps and the location of errors in models. *Acta Crystallog. sect. A*, **47**, 392-400.
20. Richardson, J. S. (1981). The anatomy and taxonomy of protein structure. *Advan. Protein Chem.* **34**, 167-339.
21. Matthews, B. W. (1968). Solvent content of protein crystals. *J. Mol. Biol.* **33**, 491-497.
22. Janin, J. & Rodier, F. (1995). Protein-protein interaction at crystal contacts. *Proteins: Struct. Funct. Genet.* **23**, 580-587.
23. Jäger, J., Moser, M., Sauder, U. & Jansonius, J. N. (1994). Crystal structures of *Escherichia coli* aspartate aminotransferase in two conformations. *J. Mol. Biol.* **239**, 285-305.
24. Goldberg, J. M., Swanson, R. V., Goodman, H. S. & Kirsch, J. F. (1991). The tyrosine-225 to phenylalanine mutation of *Escherichia coli* aspartate aminotransferase results in an alkaline transition in the spectrophotometric and kinetic pK_a values and reduced values of both k_{cat} and K_m. *Biochemistry*, **30**, 305-312.
25. di Salvo, M. L., Delle Fratte, S., De Biase, D., Bossa, F. & Schirch, V. (1998). Purification and characterization of recombinant rabbit cytosolic serine hydroxymethyltransferase. *Protein Express. Purif.* **13**, 177-183.

26. Yang, E. S. & Schirch, V. (2000). Tight binding of pyridoxal 5′-phosphate to recombinant *Escherichia coli* pyridoxine 5′-phosphate oxidase. *Arch. Biochem. Biophys.* 377, 109-114.
27. Collaborative Computing Project No 4. (1994). The CCP4 suite: programs for protein crystallography. *Acta Crystallog. sect. D*, 50, 760-763.
28. Brunger, A. T., Adams, P. D., Clore, G. M., DeLano, W. L., Gros, P., Grosse-Kunstleve, R. W. *et al.* (1998). Crystallography & NMR System: a new software suite for macromolecular structure determination. *Acta Crystallog. sect. D*, 54, 905-921.
29. Brunger, A. T. (1992). Free *R*-value: a novel statistical quantity for assessing the accuracy of crystal structures. *Nature*, 35, 42-475.
30. Kraulis, P. J. (1991). MOLSCRIPT: a program to produce both detailed and schematic plots of protein structures. *J. Appl. Crystallog.* 24, 946-950.
31. Merrit, E. A. & Murphy, M. E. P. (1994). Raster3D version 2.0: a program for photorealistic molecular graphics. *Acta Crystallog. sect. D*, 50, 869-873.
32. Esnouf, R. M. (1997). An extensively modified version of MolScript that includes greatly enhanced coloring capabilities. *J. Mol. Graph.* 15, 132-134.
33. Nicholls, A., Sharp, K. A. & Honig, B. (1991). Protein folding and association: insights from the interfacial and thermodynamic properties of hydrocarbons. *Proteins: Struct. Funct. Genet.* 11, 281-296.

Edited by R. Huben

(Received 2 August 2001; received in revised form 2 November 2001; accepted 6 November 2001)